

Super Fast Beam Tracking in Phased Antenna Arrays

Jiahui Li*, Yin Sun[§], Limin Xiao^{¶‡}, Shidong Zhou*, C. Emre Koksali[†]

*Dept. of EE, [¶]Research Institute of Information Technology, Tsinghua University, Beijing, 100084, China

[§]Dept. of ECE, Auburn University, Auburn AL, 36849, U.S.A.

[†]Dept. of ECE, The Ohio State University, Columbus OH, 43210, U.S.A.

Abstract

The directionality of millimeter-wave (mmWave) communications creates a significant challenge in serving fast-moving mobile terminals on, e.g., high-speed vehicles, trains, and UAVs. This challenge is exacerbated in mmWave systems using analog antenna arrays, because of the inherent non-convexity in the control of the phase shifters. In this paper, we develop a recursive beam tracking algorithm which can simultaneously achieve fast tracking speed, high tracking accuracy, low complexity, and low pilot overhead. In static scenarios, this algorithm converges to the minimum Cramér-Rao lower bound (CRLB) of beam tracking with high probability. In dynamic scenarios, even at SNRs as low as 0dB, our algorithm is capable of tracking a mobile moving at an angular velocity of 10-20 degrees per second, using only 5 pilot symbols per second. If combining with a simple TDMA pilot pattern, this algorithm can track hundreds of high-speed mobiles in 5G configurations. Our simulations show that the tracking performance of this algorithm is much better than several state-of-the-art algorithms. The key analytical tools used in our algorithm design are stochastic approximation and recursive estimation with a control parameter.

A part of this paper will be presented in the 2017 51st Asilomar Conference on Signals, Systems, and Computers [1].

[‡]Corresponding author.

This work was supported in part by ONR grant N00014-17-1-2417, National Basic Research Program of China (973 Program) grant 2012CB316002, National S&T Major Project grant 2017ZX03001011-002, National Natural Science Foundation of China grant 61631013, National High Technology Research and Development Program of China (863 Program) grant 2014AA01A703, Science Fund for Creative Research Groups of NSFC grant 61321061, Tsinghua University Initiative Scientific Research grant 2016ZH02-3, International Science and Technology Cooperation Program grant 2014DFT10320, Tsinghua-Qualcomm Joint Research Program, and Huawei HIRP project.

I. INTRODUCTION

The explosively growing data traffic in future wireless systems can be leveraged by using higher frequency bands, e.g., millimeter-wave (mmWave) [2]–[4]. In the mmWave band, the scattering effect is very weak [5], [6], therefore we only need to estimate the multipath channel along several distinctive directions, i.e., the line-of-sight path and a few relatively strong reflected paths. For each path, the angular spread is very small [5], [6], therefore it is critical for a mmWave receiver to track these rare and precious paths accurately under mobile conditions. Since the large scale antenna array with high array gain is needed to compensate the large propagation loss in the mmWave band [2], [5], the resulting narrow beams will make accurate beam direction tracking more crucial.

Moreover, as the array size grows and the carrier frequency increases, the large number of A/D (or D/A) converters in the fully digital array tends to make the design infeasible due to high energy consumption and huge hardware cost [4]. One of the most economical solutions is analog beamforming [4], [7]–[11], in which the signals of all antennas are beamformed in the analog domain by using phase shifters, and a single A/D (or D/A) is used for digital processing. This analog beamforming solution has been standardized by IEEE 802.11ad [12] and IEEE 802.15.3c [13], and is actively discussed by several 5G industrial organizations [14], [15].

Since only one observation is obtained at one time for each analog beamforming array, one fundamental challenge in analog beamforming is how to accurately track the dynamic beam directions using limited pilot resources. This challenge is especially difficult when a huge number of beams need to be tracked, which come from many different terminals and reflectors with high mobility. Typical scenarios include vehicle-to-vehicle/infrastructure (V2V/V2I) [16], high-speed railway [17], and unmanned aerial vehicle (UAV) [18], etc. This challenge has also been recognized in the industry as one important research task for 5G mmWave and massive MIMO systems, e.g., [19]–[23].

A. Related Work

There has been a large number of studies on beam direction estimation/tracking in mmWave systems with analog beamforming arrays. We first review the state-of-the-art algorithms:

- **Beam estimation:** This kind of methods sweep the channel with several spatial beams and estimates the beam directions of the channel based on these observations. According to different sweeping methods, we divide them into three categories: 1) Exhaustive

sweeping [24]–[26]: Narrow spatial beams are used to scan the channel exhaustively. 2) Hierarchical multi-resolution sweeping [18], [27]–[30]: The hierarchical multi-resolution codebooks are used to sweep the channel. 3) Random sweeping [31]–[33]: Several random analog beamforming vectors are used to observe the channel. Here the exhaustive sweeping methods can guarantee a thorough observation on the channel, but the pilot training overhead increases linearly with the number of antennas, which will easily go beyond the limitation of transmission resource. Compared with the exhaustive sweeping methods, the latter two categories can reduce the pilot overhead a lot. However, all the above algorithms do not design the optimal analog beamforming vectors according to the channel directions, which causes a waste of transmission energy and will introduce some losses to the estimation accuracy.

- **Beam tracking:** This kind of methods take the prior information of beam directions into account. In [34]–[37], the estimated beam direction will be updated based on the latest estimation. However, the analog beamforming vectors during pilot training in these algorithms are not well-designed, which wastes much transmission energy and will also introduce some losses to the estimation accuracy. In [38], the authors start to study the optimization of analog beamforming vectors during pilot training, which can be obtained based on the latest estimation. However, its beam direction estimation is done independently without using the historical estimation information. Moreover, it is worth highlighting that none of these works study the convergence property of the beam tracking algorithms, which may cause these algorithms to converge to the wrong beam direction.

It can be observed that all the existing algorithms have certain shortcomings. In particular, the poor pilot training scheme will result in high pilot overhead and low estimation accuracy, and the inappropriate estimation method may even lead to the wrong estimation.

B. Our Results

In this paper, to handle the problems mentioned above, we aim to develop an efficient beam tracking algorithm that can achieve **high** accuracy for tracking a **large number** of **high-speed** mobiles with **low** pilot overhead.¹ The detailed results and contributions of this paper are summarized as follows:

¹Note that these beams may come from either the same terminal or different terminals. For each terminal, the base station should keep track of several different beams to overcome the negative effect of channel blockage on some of the beam directions. In this paper, we will focus on the tracking problem.

TABLE I
MAXIMUM ANGULAR VELOCITY (IN degrees per second) FOR ACHIEVING 95% OF THE CHANNEL CAPACITY WITH
DIFFERENT ALGORITHMS.

SNR without array gain	Number of antennas	Recursive beam tracking	IEEE 802.11ad [12]	Least square [39]	Compressed sensing [31]–[33]
10dB	$M = 8$	18.33	—	4.13	2.29
	$M = 32$	4.18	0.06	0.29	0.57
	$M = 128$	1.03	0.23	0.03	0.11
0dB	$M = 8$	13.18	—	—	—
	$M = 32$	3.84	—	—	—
	$M = 128$	0.97	—	—	—
−5dB	$M = 8$	—	—	—	—
	$M = 32$	2.98	—	—	—
	$M = 128$	0.92	—	—	—

1. The notation “—” denotes that the corresponding algorithm cannot achieve 95% of the channel capacity even at zero angular velocity.
2. We assume that the SNR is the same for pilot training and data transmission, and 5 uniformly inserted pilot symbols per second are used for beam tracking.

- We use the stochastic Newton’s method to design a recursive beam tracking algorithm, which aims to simultaneously achieve fast tracking speed, high tracking accuracy, low complexity, and low pilot overhead.
- In *static* beam tracking scenarios, the convergence and asymptotic optimality of our algorithm are established in three steps: First, we prove that it converges to a set of beam directions with probability one, including the real beam direction and some sub-optimal beam directions (Theorem 1). Second, we prove that under certain conditions, it converges to the real beam direction, instead of other sub-optimal beam directions, with high probability (Theorem 2). Finally, if the step-size parameters are chosen appropriately, then the mean square error (MSE) of this algorithm converges to the minimum Cramér-Rao lower bound (CRLB)², and hence the highest convergence rate is achieved (Theorem 3). To the extent of our knowledge, this paper presents the first theoretical analysis on the convergence and asymptotic optimality of analog beam tracking problem.
- Simulation results in both *static* and *dynamic* beam tracking scenarios suggest that this algorithm can achieve much **lower** beam tracking error and **higher** data rate than several state-of-the-art algorithms [12], [31]–[33], [39] with the same amount of pilot overhead.

The performance of several beam tracking algorithms is summarized in Table I: One can observe that the maximum trackable angular velocity of the proposed algorithm to achieve 95% capacity is much higher than those of other algorithms, and more importantly, when SNR is equal

²The CRLB is a function of the beamforming control action. The minimum CRLB is obtained by optimizing among all control actions (see Section III-B).

to or lower than 0dB, the proposed algorithm still works well under most of the conditions, while other algorithms cannot meet the 95% capacity requirement even if the moving speed is zero. Hence, the proposed algorithm can achieve a much faster beam tracking speed than the other algorithms, over a wide range of SNR values.

In particular, if 5 uniformly inserted pilot symbols per second are used and the receive SNR of each antenna is 10 dB (or 0 dB), the proposed algorithm can track a narrow beam rotating at an angular velocity of **18.33°/s** (or **13.18°/s**), which is **72 mph** (or **52 mph**) if the mobile transmitters/reflectors steering these beams are at a distance of 100 meters. In 5G systems, one possible choice for the duration of each time-slot is 0.2 ms (i.e., one transmission time interval (TTI) [40], [41]). If 1 pilot symbol is allocated in each time-slot, then, by using a TDMA round-robin pilot pattern, one can simultaneously track **1000** high-speed mobiles such that 5 pilot symbols are inserted in a second for each mobile. And when it is needed to track extremely fast mobiles, one can insert more pilot symbols for each mobile. Hence, the tracking speed can be **very fast**.

Two major technical reasons why our algorithm achieves a good tracking performance are: 1) the probing beamforming direction in each time-slot is close to the real direction, while the other algorithms (e.g., least square [39] and compressed sensing [31]–[33]) probe a lot of beam directions, and 2) an optimal step-size is chosen to ensure a fast convergence rate to the *global optimal* beam direction, instead of other local optimal beam directions.

The rest of this paper is organized as follows. In Sections II, the system model is described. In Sections III, we formulate the beam tracking problem and obtain its performance bound. In Section IV and V, a recursive beam tracking algorithm is designed, which is proven to converge to the minimum CRLB in *static* beam tracking scenarios. In Section VI, numerical results show that this algorithm converges very fast to the minimum CRLB in the *static* beam tracking scenarios and achieves a better tradeoff curve between MSE (or data rate) vs. angular velocity in *dynamic* beam tracking scenarios.

II. MODEL DESCRIPTION

A. Notations

Lower case letters such as a and \mathbf{a} will be used to represent scalars and column vectors, respectively, where $|a|$ denotes the modulus of a and $\|\mathbf{a}\|_2$ denotes the 2-norm of \mathbf{a} . Upper case letters such as \mathbf{A} will be utilized to denote matrices. For a vector \mathbf{a} or a matrix \mathbf{A} , its transpose

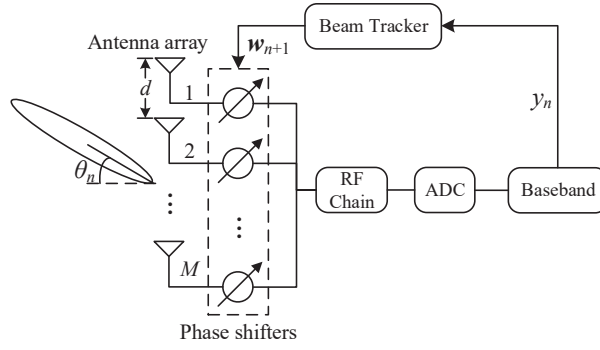


Fig. 1. System model.

is denoted by \mathbf{a}^T or \mathbf{A}^T , and its Hermitian transpose is denoted by \mathbf{a}^H or \mathbf{A}^H . Let $\mathcal{CN}(u, \sigma^2)$ stand for the circular symmetric complex Gaussian distribution with mean u and variance σ^2 , and $\mathcal{N}(u, \sigma^2)$ stand for the real Gaussian distribution with mean u and variance σ^2 . The sets of integers and real numbers are written as \mathbb{Z} and \mathbb{R} , respectively. Expectation is denoted by $\mathbb{E}[\cdot]$ and the real (imaginary) part of a variable x is denoted by $\text{Re}\{x\}$ ($\text{Im}\{x\}$). The natural logarithm of x is denoted by $\log(x)$. The phase of a complex number z is obtained by $\angle z$.

B. System Model

Consider a receiver with a linear antenna array in Fig. 1, where M antennas are placed along a line, with a distance d between neighboring antennas. The antennas are connected by phase shifters to a single radio frequency (RF) chain, and the phase shifters are controlled digitally to steer the beam. In time-slot n , a narrow-beam pilot signal p_n arrives at the antenna array from an angle-of-arrival (AoA) $\theta_n \in [-\pi/2, \pi/2]$. Hence, the channel response is $\mathbf{h}(x_n) = \beta \mathbf{a}(x_n)$, where

$$\mathbf{a}(x_n) = \left[1, e^{j\frac{2\pi d}{\lambda}x_n}, \dots, e^{j\frac{2\pi d}{\lambda}(M-1)x_n} \right]^H, \quad (1)$$

is the steering vector, $x_n = \sin(\theta_n)$ is the sine of the AoA θ_n , λ is the wavelength, and β is the complex channel response at the first antenna.

Let $w_{mn} \in [-\pi, \pi]$ be the phase shift in radians provided by the m -th phase shifter in time-slot n . Then, the analog beamforming vector steered by the phase shifters is

$$\mathbf{w}_n = \frac{1}{\sqrt{M}} \left[e^{jw_{1n}}, e^{jw_{2n}}, \dots, e^{jw_{Mn}} \right]^H. \quad (2)$$

Combining the output signals of the phase shifters yields

$$r_n = \mathbf{w}_n^H [\beta \mathbf{a}(x_n)] p_n + \sigma z_n, \quad (3)$$

where σ^2 is the noise power at each antenna, and the z_n 's are *i.i.d.* circularly symmetric complex Gaussian random variables with zero mean and unity variance. Without losing information, we can divide r_n in (3) by $p_n\beta$, the observation that contains the beam direction information is obtained as

$$y_n = \mathbf{w}_n^H \mathbf{a}(x_n) + \frac{z_n}{\sqrt{\rho}}, \quad (4)$$

where $\rho = |p_n\beta|^2/\sigma^2$ is the SNR at each antenna. Given x_n and \mathbf{w}_n , the conditional probability density function of y_n is

$$p(y_n|x_n, \mathbf{w}_n) = \frac{\rho}{\pi} e^{-\rho|y_n - \mathbf{w}_n^H \mathbf{a}(x_n)|^2}. \quad (5)$$

A beam tracker determines the analog beamforming vector \mathbf{w}_n and provides an estimate \hat{x}_n of the sine x_n of the AoA after applying \mathbf{w}_n .³ From a control system perspective, x_n is the system state, \hat{x}_n is the estimate of the system state, the beamforming vector \mathbf{w}_n is the control action, and y_n is a noisy observation that is determined by a non-linear and non-convex function of the system state x_n and control action \mathbf{w}_n .

Let $\psi = (\mathbf{w}_1, \mathbf{w}_2, \dots, \hat{x}_1, \hat{x}_2, \dots)$ represent a beam tracking policy. In particular, we consider the set Ψ of *causal* beam tracking policies: The estimate \hat{x}_n of time-slot n and the control action \mathbf{w}_{n+1} of time-slot $n+1$ are determined by using the history of the control actions $(\mathbf{w}_1, \dots, \mathbf{w}_n)$ and the observations (y_1, \dots, y_n) . The policy ψ is to be designed in a beam tracking problem for a better tracking performance, e.g., convergence rate and beam tracking error. In the next section, we will formulate this beam tracking problem.

III. BEAM TRACKING AND ITS PERFORMANCE BOUND

In Section III-A, we first formulate the beam tracking problem. Then, in Section III-B, we derive a fundamental performance bound for the beam tracking problem.

A. Problem Formulation

³Interestingly, by tracking the sine x_n , we obtain a beam tracking algorithm with better robustness than tracking the AoA θ_n ; see Section V-C for details.

Our objective is to develop a beam tracking algorithm to minimize the beam tracking error in each time-slot. Given any time-slot n , the beam tracking problem can be formulated as

$$\text{MSE}_{\text{opt},n} \triangleq \min_{\psi \in \Psi} \mathbb{E} [(\hat{x}_n - x_n)^2] \quad (6)$$

$$\text{s.t. } \mathbb{E} [\hat{x}_n] = x_n, \quad (7)$$

$$(1), (2), (4),$$

where $\text{MSE}_{\text{opt},n}$ is the optimum value of (6), and the constraint (7) ensures that \hat{x}_n is an *unbiased* estimate of x_n . Problem (6) is a constrained sequential control and estimation problem that is difficult, if not impossible, to solve optimally. First, the system is partially observed through the observation y_n . Second, both the control action \mathbf{w}_n and the estimate \hat{x}_n need to be optimized in Problem (6): On the one hand, because only the phase shifts (w_{1n}, \dots, w_{Mn}) in (2) are controllable, the optimal control of \mathbf{w}_n is a non-convex optimization problem. On the other hand, as shown in Fig. 3 and (27) below, the optimization of the estimate \hat{x}_n is also non-convex and there are multiple local optimal estimates.

B. Fundamental Lower Bound of Beam Tracking Error

Next, we establish a lower bound of $\text{MSE}_{\text{opt},n}$ defined in (6) under the *static* beam tracking scenarios, where $x_n = x$ for all time-slot n . Given the control actions $(\mathbf{w}_1, \dots, \mathbf{w}_n)$, the MSE is lower bounded by the CRLB [42]

$$\mathbb{E} [(\hat{x}_n - x)^2] \geq \frac{1}{\sum_{i=1}^n I(x, \mathbf{w}_i)}, \quad (8)$$

where $I(x, \mathbf{w}_i)$ is the Fisher information [43] that can be computed by using (5):

$$\begin{aligned} I(x, \mathbf{w}_i) &= \mathbb{E} \left[-\frac{\partial^2 \log p(y_i | x, \mathbf{w}_i)}{\partial x^2} \middle| x, \mathbf{w}_i \right] \\ &= \frac{2\rho}{M} \left| \sum_{m=1}^M \frac{2\pi d}{\lambda} (m-1) e^{j[w_{mi} - \frac{2\pi d}{\lambda}(m-1)x]} \right|^2. \end{aligned} \quad (9)$$

Note that the Fisher information $I(x, \mathbf{w}_i)$ is the function of \mathbf{w}_i . By optimizing the control actions $(\mathbf{w}_1, \dots, \mathbf{w}_n)$ in the right-hand-side (RHS) of (8), we obtain

$$\frac{1}{n} \sum_{i=1}^n I(x, \mathbf{w}_i) \leq \frac{2M(M-1)^2 \pi^2 d^2 \rho}{\lambda^2} \triangleq I_{\max}, \quad (10)$$

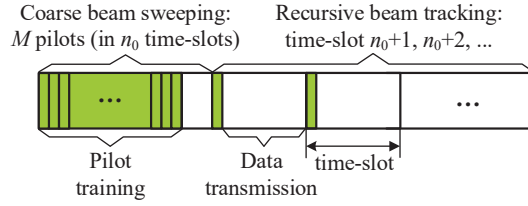


Fig. 2. Frame structure.

where the maximum Fisher information I_{\max} in (10) is achieved if, and only if, for $i = 1, \dots, n$

$$\mathbf{w}_i = \frac{\mathbf{a}(x)}{\sqrt{M}} = \frac{1}{\sqrt{M}} \left[1, e^{j\frac{2\pi d}{\lambda}x}, \dots, e^{j\frac{2\pi d}{\lambda}(M-1)x} \right]^H. \quad (11)$$

Hence, $\text{MSE}_{\text{opt},n}$ in (6) is lower bounded by the minimum CRLB

$$\text{MSE}_{\text{opt},n} \geq \frac{1}{nI_{\max}}. \quad (12)$$

In what follows, we will investigate a new recursive analog beam tracking algorithm that can achieve this lower bound.

IV. RECURSIVE ANALOG BEAM TRACKING ALGORITHM

In this section, we first introduce our new recursive analog beam tracking algorithm. Then, we will show how to use the stochastic Newton's method to obtain this algorithm.

A. Algorithmic Framework

We first introduce the frame structure of the transmitted signals. The transmission is divided into two stages: 1) coarse beam sweeping and 2) recursive beam tracking. As depicted in Fig. 2, M pilots will be sent successively in *Stage 1*, which is assumed to be finished by the end of time-slot n_0 ($n_0 \geq 1$) and to obtain an initial estimate \hat{x}_{n_0} . In *Stage 2*, one pilot is allocated in each time-slot (e.g., at the beginning of each time-slot as in Fig. 2), and the estimate \hat{x}_n as well as the control action \mathbf{w}_n are updated recursively to realize an accurate tracking performance.

Then, based on this frame structure, we design a recursive analog beam tracking algorithm as described in Algorithm 1.

B. Rationale Behind Algorithm Design

In this subsection, we will clarify how Algorithm 1 is designed. Due to the non-convex property of the beam tracking problem in (6), a good initial estimate \hat{x}_{n_0} obtained in *Stage 1* is quite important for the success of tracking the real direction x_n in *Stage 2*. As depicted in Fig.

Algorithm 1 Recursive Analog Beam Tracking

- 1) **Coarse Beam Sweeping:** Transmit M pilots successively in the first $n_0 \geq 1$ time-slots. The analog beamforming vector $\tilde{\mathbf{w}}_m$ for receiving the m -th training signal \tilde{y}_m is

$$\tilde{\mathbf{w}}_m = \frac{\mathbf{a}\left(\frac{2m}{M} - \frac{M+1}{M}\right)}{\sqrt{M}}, m = 1, \dots, M. \quad (13)$$

Obtain the initial estimate \hat{x}_{n_0} of the beam direction by

$$\hat{x}_{n_0} = \arg \max_{\hat{x} \in \mathcal{X}} \left| \mathbf{a}(\hat{x})^H \cdot \sum_{m=1}^M \tilde{y}_m \tilde{\mathbf{w}}_m \right|, \quad (14)$$

where $\mathcal{X} = \left\{ \frac{1-M_0}{M_0}, \frac{3-M_0}{M_0}, \dots, \frac{M_0-1}{M_0} \right\}$.

- 2) **Recursive Beam Tracking:** In each time-slot $n = n_0+1, n_0+2, \dots$, the analog beamforming vector \mathbf{w}_n is

$$\mathbf{w}_n = \frac{\mathbf{a}(\hat{x}_{n-1})}{\sqrt{M}}. \quad (15)$$

The estimate \hat{x}_n of the beam direction is updated by

$$\hat{x}_n = [\hat{x}_{n-1} - a_n \operatorname{Im}\{y_n\}]_{-1}^1, \quad (16)$$

where $[x]_b^c = \max\{\min\{x, c\}, b\}$ and $a_n > 0$ is the step-size that will be specified later.

3, we can conjecture that a good initial estimate \hat{x}_{n_0} should be within the mainlobe set $\mathcal{B}(x_{n_0})$, defined by

$$\mathcal{B}(x_{n_0}) = \left(x_{n_0} - \frac{\lambda}{Md}, x_{n_0} + \frac{\lambda}{Md} \right) \cap [-1, 1]. \quad (17)$$

To achieve this goal, the exhaustive sweeping is used to thoroughly observe the channel (i.e., by using the beamforming vectors in (13)), and then motivated by the orthogonal matching pursuit method (e.g., [32]), we use (14) to obtain the initial estimate \hat{x}_{n_0} from these observations, where the size M_0 of the dictionary \mathcal{X} determines the estimation resolution and a larger M_0 provides a more accurate estimate. Our simulations suggest that, if the SNR $\rho \geq 0$ dB and $M_0 = 2M$, a good initial estimate \hat{x}_{n_0} within the mainlobe $\mathcal{B}(x_{n_0})$ can be obtained with a probability higher than 99.99%.⁴

In *Stage 2*, the recursive beam tracker in (16) is motivated by the following maximum

⁴One can use more time-slots (pilot resources) to support lower SNR in *Stage 1*. As *Stage 1* is executed only once, this will not increase the total pilot overhead by much.

likelihood (ML) estimator:

$$\max_{\hat{x}_n \in [-1, 1]} \left\{ \max_{\mathbf{w}_n} \mathbb{E} \left[\log p(y_n | \hat{x}_n, \mathbf{w}_n) \mid \hat{x}_n, \mathbf{y}^{n-1}, \mathbf{W}^n \right] \right\}, \quad (18)$$

given the observations $\mathbf{y}^{n-1} = (y_1, \dots, y_{n-1})$ of the first $n-1$ time-slots and the control actions $\mathbf{W}^n = (\mathbf{w}_1, \dots, \mathbf{w}_n)$ of the first n time-slots, where \mathbf{w}_n is subject to (2). We propose a two-layer nested optimization algorithm to solve (18):

In the inner layer, to achieve the maximum value, it is equivalent to maximize the Fisher information to find the best control action \mathbf{w}_n as follows:

$$\begin{aligned} \max_{\mathbf{w}_n} I(\hat{x}_{n-1}, \mathbf{w}_n) \\ \text{s.t. (2).} \end{aligned} \quad (19)$$

According to (10), the solution of (19) is given by $\mathbf{w}_n = \mathbf{a}(\hat{x}_{n-1})/\sqrt{M}$, i.e., (15).

In the outer layer, rather than directly solving (18), we propose to use the stochastic Newton's method, given by [42]

$$\begin{aligned} \hat{x}_n &= \left[\hat{x}_{n-1} - s_n \cdot \frac{\frac{\partial \log p(y_n | \hat{x}_{n-1}, \mathbf{w}_n)}{\partial \hat{x}_{n-1}}}{\mathbb{E} \left[\frac{\partial^2 \log p(y_n | \hat{x}_{n-1}, \mathbf{w}_n)}{\partial \hat{x}_{n-1}^2} \mid \hat{x}_{n-1}, \mathbf{w}_n \right]} \right]_{-1}^1 \\ &= \left[\hat{x}_{n-1} + s_n \cdot \frac{\frac{\partial \log p(y_n | \hat{x}_{n-1}, \mathbf{w}_n)}{\partial \hat{x}_{n-1}}}{I(\hat{x}_{n-1}, \mathbf{w}_n)} \right]_{-1}^1, \end{aligned} \quad (20)$$

where s_n is the step-size, $[x]_{-1}^1 = \max\{\min\{x, 1\}, -1\}$ constrains the estimation within the feasible region $[-1, 1]$,

$$\frac{\partial \log p(y_n | \hat{x}_{n-1}, \mathbf{w}_n)}{\partial \hat{x}_{n-1}} = 2\rho \operatorname{Re} \left\{ [y_n - \mathbf{w}_n^H \mathbf{a}(\hat{x}_{n-1})]^H \cdot \mathbf{w}_n^H \frac{\partial \mathbf{a}(\hat{x}_{n-1})}{\partial \hat{x}_{n-1}} \right\}, \quad (21)$$

and

$$I(\hat{x}_{n-1}, \mathbf{w}_n) = \frac{2\rho}{M} \left| \sum_{m=1}^M \frac{2\pi d}{\lambda} (m-1) e^{j[w_{mn} - \frac{2\pi d}{\lambda} (m-1)\hat{x}_{n-1}]} \right|^2. \quad (22)$$

By plugging (15), (21) and (22) into (20), we can obtain the recursive beam tracker as

$$\hat{x}_n = \left[\hat{x}_{n-1} - \frac{\lambda s_n}{\sqrt{M}(M-1)\pi d} \cdot \operatorname{Im}\{y_n\} \right]_{-1}^1. \quad (23)$$

Let $a_n = \lambda s_n / [\sqrt{M}(M-1)\pi d]$ in (23) be the new step-size, then we can obtain (16). Hence,

even though the original algorithm in (20) is quite complicated, we are able to simplify it significantly, which greatly reduces the computational complexity of the algorithm.

V. ASYMPTOTIC OPTIMALITY ANALYSIS

In this section, we first present the key challenge faced by Algorithm 1. Then, a series of three theorems will be developed to prove its asymptotic optimality, which helps resolve this challenge. Finally, we will investigate an alternative scheme that can be used to perform beam tracking.

A. Multiple Stable Points for Recursive Procedure

To obtain the points that the recursive procedure (15) and (16) might converge to, we will introduce its corresponding ordinary differential equation (ODE). Using (4) and (15), the recursive beam tracker in (16) can also be expressed as

$$\hat{x}_n = \left[\hat{x}_{n-1} + a_n \left(f(\hat{x}_{n-1}, x) - \frac{\text{Im}\{z_n\}}{\sqrt{\rho}} \right) \right]_{-1}^1, \quad (24)$$

where function $f : \mathbb{R} \times \mathbb{R} \mapsto \mathbb{R}$ is defined as

$$f(v, x) \triangleq -\frac{1}{\sqrt{M}} \text{Im} \{ \mathbf{a}(v)^H \mathbf{a}(x) \}. \quad (25)$$

This recursive procedure can be seen as a noisy, discrete-time approximation of the following ODE [44, Section 2.1]

$$\frac{d\hat{x}(t)}{dt} = \begin{cases} \max\{f(-1, x), 0\} & \text{if } \hat{x}(t) = -1 \\ f(\hat{x}(t), x) & \text{if } -1 < \hat{x}(t) < 1 \\ \min\{f(1, x), 0\} & \text{if } \hat{x}(t) = 1, \end{cases} \quad (26)$$

with $t \geq 0$ and $\hat{x}(0) = \hat{x}_{n_0}$. According to [44], [45], the recursive procedure will converge to one of the stable points of the ODE (26). Here the stable point of the ODE (26) is defined as a point v_0 that satisfies $f(v_0, x) = 0$ and $f'_v(v_0, x) < 0$, which means that any starting point from a certain neighbourhood of v_0 will make the ODE converge to v_0 itself.

As depicted in Fig. 3, $f(v, x)$ is not monotonic in v (i.e., Problem (6) is non-convex), and within each lobe (i.e., the mainlobe or the sidelobe) of the antenna array pattern, there exists

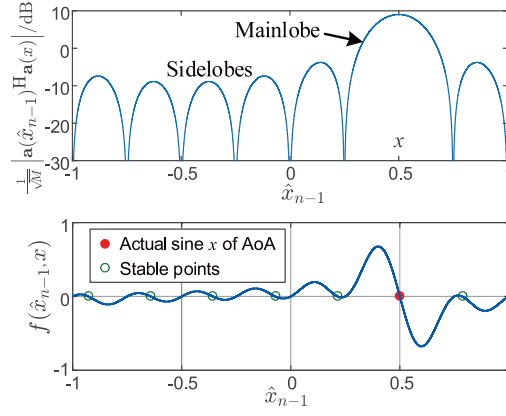


Fig. 3. $\frac{1}{\sqrt{M}} |\mathbf{a}(\hat{x}_{n-1})^H \mathbf{a}(x)|$ and $f(\hat{x}_{n-1}, x)$ vs. \hat{x}_{n-1} for $M = 8$, $x = 0.5$, $d = 0.5\lambda$. Notice that the stable points are not at the sidelobe peaks.

one stable point. The *local optimal stable points* for the recursive procedure is given by

$$\begin{aligned} \mathcal{S}(x) &= \{v \in (-1, 1] : f(v, x) = 0, f'_v(v, x) < 0\} \\ &= \left\{ v_k \in (-1, 1] : v_k = x + \frac{k\lambda}{(M-1)d}, k \in \mathbb{Z} \right\}. \end{aligned} \quad (27)$$

Note that except for x , the antenna array gain is quite low at other local optimal stable points in $\mathcal{S}(x)$, where the loss of antenna array gain is nearly 20dB and will be higher if more antennas are configured. Hence, one key challenge is *how to ensure that Algorithm 1 converges to the real direction x , instead of other local optimal stable points in $\mathcal{S}(x)$?*

B. Step-size Design and Asymptotic Optimality Analysis

In *static* beam tracking, we adopt the widely used diminishing step-sizes, given by [42], [44], [45]

$$a_n = \frac{\alpha}{n - n_0 + N_0}, \quad n = n_0 + 1, n_0 + 2, \dots, \quad (28)$$

where $\alpha > 0$ and $N_0 \geq 0$.

We use the stochastic approximation and recursive estimation theory [42], [44], [45] to analyze Algorithm 1. In particular, we now develop a series of three theorems to resolve the challenge mentioned in Section V-A.

Theorem 1 (Convergence to Stable Points). If a_n is given by (28) with any $\alpha > 0$ and $N_0 \geq 0$, then \hat{x}_n converges to a unique point within $\mathcal{S}(x) \cup \{-1\} \cup \{1\}$ with probability one.

Proof. See Appendix A. □

Hence, for general step-size parameters α and N_0 in (28), \hat{x}_n converges to a stable point in $\mathcal{S}(x)$ or a boundary point.

Theorem 2 (Convergence to the Real Direction x). If (i) the initial point satisfies $\hat{x}_{n_0} \in \mathcal{B}(x)$, (ii) a_n is given by (28) with any $\alpha > 0$, then there exist $N_0 \geq 0$ and $C(\hat{x}_{n_0}) > 0$ such that

$$P(\hat{x}_n \rightarrow x | \hat{x}_{n_0} \in \mathcal{B}(x)) \geq 1 - 2e^{-C(\hat{x}_{n_0})\frac{\rho}{\alpha^2}}. \quad (29)$$

Proof Sketch. Motivated by Chapter 4 of [44], we will prove this theorem in three steps: in *Step 1*, we will construct two continuous processes based on the discrete process $\{\hat{x}_n\}$; in *Step 2*, using these continuous processes, we form a sufficient condition for the convergence of the discrete process $\{\hat{x}_n\}$; in *Step 3*, we will derive the probability lower bound for this condition, which is also a lower bound for $P(\hat{x}_n \rightarrow x | \hat{x}_{n_0} \in \mathcal{B}(x))$. See Appendix B for the details. \square

By Theorem 2, if the initial point \hat{x}_{n_0} is in the mainlobe \mathcal{B} , the probability that \hat{x}_n does not converge to x decays *exponentially* with respect to ρ/α^2 . Hence, one can increase the SNR ρ and reduce the step-size parameter α to ensure $\hat{x}_n \rightarrow x$ with high probability. Under the condition of $\rho = 10\text{dB}$ and $M = 8\text{-}128$, typical values of N_0 required by the sufficient condition in Theorem 2 are 10-50. However, one can choose any $N_0 \geq 0$ to achieve a sufficiently high probability of $\hat{x}_n \rightarrow x$ in simulations.

Theorem 3 (Convergence to x with the Minimum MSE). If (i) a_n is given by (28) with

$$\alpha = \frac{\lambda}{\sqrt{M}(M-1)\pi d} \triangleq \alpha^*, \quad (30)$$

and any $N_0 \geq 0$, and (ii) $\hat{x}_n \rightarrow x$, then

$$\sqrt{n}(\hat{x}_n - x) \xrightarrow{d} \mathcal{N}(0, I_{\max}^{-1}), \quad (31)$$

as $n \rightarrow \infty$, where \xrightarrow{d} represents convergence in conditional distribution given $\hat{x}_n \rightarrow x$, and I_{\max} is defined in (10). In addition,

$$\lim_{n \rightarrow \infty} n \mathbb{E}[(\hat{x}_n - x)^2 | \hat{x}_n \rightarrow x] = I_{\max}^{-1}. \quad (32)$$

Proof. See Appendix C. \square

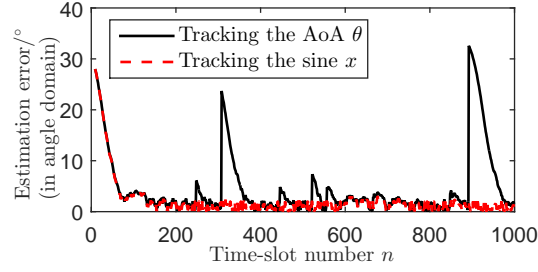


Fig. 4. Estimation error comparison between the algorithms tracking the AoA θ and its sine x .

Theorem 3 tells us that α should not be too small: If $\alpha = \alpha^*$ in (30), then the minimum CRLB on the RHS of (12) is achieved asymptotically with high probability, which ensures the highest convergence rate⁵. In practice, we suggest to choose $\alpha = \alpha^*$ and $N_0 = 0$ in (28). Interestingly, Theorem 3 can be readily generalized to the track of any smooth function of x :

Corollary 1. If the conditions of Theorem 3 are satisfied, then for any first-order differentiable vector function $\mathbf{u}(x)$

$$\lim_{n \rightarrow \infty} n \mathbb{E} \left[\|\mathbf{u}(\hat{x}_n) - \mathbf{u}(x)\|_2^2 \mid \hat{x}_n \rightarrow x \right] = \|\mathbf{u}'(x)\|_2^2 I_{\max}^{-1}. \quad (33)$$

Proof. See Appendix D. □

For example, consider the channel response $\mathbf{h}(x) = \beta \mathbf{a}(x)$. If $\alpha = \alpha^*$ and $N_0 = 0$, Corollary 1 tells us that, with a high probability, the minimum CRLB of $\mathbf{h}(x)$ is achieved in the following limit:

$$\begin{aligned} & \lim_{n \rightarrow \infty} n \mathbb{E} \left[\|\mathbf{h}(\hat{x}_n) - \mathbf{h}(x)\|_2^2 \mid \hat{x}_n \rightarrow x \right] \\ &= I_{\max}^{-1} \sum_{m=1}^{M-1} \left| \frac{\partial \left(\beta e^{-j \frac{2\pi d}{\lambda} m x} \right)}{\partial x} \right|^2 = \frac{(2M-1)\sigma^2}{3(M-1)}. \end{aligned} \quad (34)$$

C. Further Discussion: To Track the AoA θ or its Sine x ?

We can design the analog beam tracking algorithm by tracking either the AoA θ or its sine x . The algorithm that tracks the sine x is provided in Algorithm 1. The algorithm that directly tracks the AoA θ is described in Algorithm 2.

⁵The convergence rate is defined as the asymptotic properties of normalized errors, i.e., $\lim_{n \rightarrow \infty} n \mathbb{E} [(\hat{x}_n - x)^2]$ [46]. Algorithm 1 is capable of approaching the minimum MSE, which corresponds to the highest convergence rate.

Algorithm 2 Angular Domain Recursive Analog Beam Tracking

- 1) **Coarse Beam Sweeping:** Transmit M pilots successively in the first $n_0 \geq 1$ time-slots. The analog beamforming vector $\tilde{\mathbf{w}}_m$ for receiving the m -th training signal \tilde{y}_m is given by (13). Obtain the initial estimate $\hat{\theta}_{n_0}$ of the beam direction by

$$\hat{\theta}_{n_0} = \arcsin \left\{ \arg \max_{\hat{x} \in \mathcal{X}} \left| \mathbf{a}(\hat{x})^H \cdot \sum_{m=1}^M \tilde{y}_m \tilde{\mathbf{w}}_m \right| \right\}. \quad (35)$$

- 2) **Recursive Beam Tracking:** In each time-slot $n = n_0 + 1, n_0 + 2, \dots$, the analog beamforming vector \mathbf{w}_n is

$$\mathbf{w}_n = \frac{1}{\sqrt{M}} \mathbf{a}(\sin(\hat{\theta}_{n-1})). \quad (36)$$

The estimate $\hat{\theta}_n$ is updated by

$$\hat{\theta}_n = \left[\hat{\theta}_{n-1} - \frac{a_n}{\cos(\hat{\theta}_{n-1})} \text{Im} \{y_n\} \right]_{-\frac{\pi}{2}}^{\frac{\pi}{2}}, \quad (37)$$

where $a_n > 0$ is the step-size.

The convergence rate of Algorithm 2 can be characterized by Corollary 1 with $u(x) = \arcsin x$. In particular, Algorithm 1 and Algorithm 2 share the same asymptotic convergence rate when $\hat{\theta}_n$ is very close to θ . On the other hand, if $\hat{\theta}_{n-1}$ is close to $-\frac{\pi}{2}$ or $\frac{\pi}{2}$, $\cos(\hat{\theta}_{n-1})$ in (37) is close to zero. As a result, Algorithm 2 is not stable and may even oscillate when θ_n is close to $-\frac{\pi}{2}$ or $\frac{\pi}{2}$. However, this oscillation issue does not exist in Algorithm 1.

Figure 4 depicts the tracking errors in angular degree in both algorithms, where the system parameters are configured as: $p_n = (1 - j)/\sqrt{2}$, $\beta = (1 + j)/\sqrt{2}$, $\rho = 10\text{dB}$, $M = 8$, $d = 0.5\lambda$, $\theta = 88^\circ$, $x = \sin(\theta) \approx 0.9994$, $a_n = \alpha^*/10$. It can be observed that both algorithms have similar tracking performance at the beginning. As the estimate gets closer to the real value, Algorithm 2 that tracks the AoA θ starts to oscillate, while Algorithm 1 is stable.

In addition, (15) and (16) in Algorithm 1 are less complicated than (36) and (37) in Algorithm 2 (although both algorithms are of low complexity). Because of these reasons, we choose to track the sine x of the AoA in this paper, instead of tracking the AoA θ directly. If the AoA is needed, then one can use the arcsin function to obtain it, i.e., $\theta = \arcsin x$.

VI. NUMERICAL ANALYSIS

We compare Algorithm 1 with three reference algorithms:

- 1) *IEEE 802.11ad* [12]: This algorithm contains two stages: beam sweep and beam tracking. In the first stage, sweep the beamforming directions in the DFT codebook (13) and choose the direction with the strongest received signal as the best beam direction. In the second stage, probe the best beam direction and its two adjacent beam directions, then choose the strongest direction as the new best beam direction. The second stage is performed periodically.
- 2) *Least square* [39]: Sweep all the beamforming directions in the DFT codebook (13) and use the least square algorithm to estimate the channel response $\mathbf{h}(x_n)$. Then obtain the analog beamforming vector \mathbf{w}_n for data transmission by

$$w_{mn} = \angle \hat{h}_m(x_n), m = 1, 2, \dots, M, \quad (38)$$

where $\hat{h}_m(x_n)$ is the m -th element of the estimated channel response $\hat{\mathbf{h}}(x_n)$.

- 3) *Compressed sensing* [31]–[33]: Randomly choose the phase shifts w_{mn} from $\{\pm 1, \pm j\}$ to receive pilot signals. Then use the sparse recovery algorithm to estimate the sine of AoA x_n , where a DFT dictionary with a size of 1024 is utilized.

Two performance metrics are considered: (i) the MSE of the channel response $\mathbf{h}(x_n)$, defined by

$$\text{MSE}_{\mathbf{h},n} \triangleq \mathbb{E} \left[\left\| \hat{\mathbf{h}}(x_n) - \mathbf{h}(x) \right\|_2^2 \right], \quad (39)$$

for the least square algorithm and

$$\text{MSE}_{\mathbf{h},n} \triangleq \mathbb{E} \left[\left\| \mathbf{h}(\hat{x}_n) - \mathbf{h}(x) \right\|_2^2 \right], \quad (40)$$

for other algorithms, and (ii) the achievable rate R_n , i.e.,

$$R_n \triangleq \log_2 \left(1 + \rho |\mathbf{w}_n^H \mathbf{a}(x_n)|^2 \right). \quad (41)$$

The system parameters are configured as: $p_n = (1 - j)/\sqrt{2}$, $\beta = (1 + j)/\sqrt{2}$, $\rho = 10\text{dB}$, $M = 16$, $M_0 = 2M$, $d = 0.5\lambda$. In the following subsections, we will investigate the static beam tracking scenarios and the dynamic beam tracking scenarios separately.

A. Static Beam Tracking

In static beam tracking scenarios, we assume that one pilot is allocated in each time-slot. Hence, these algorithms have the same pilot overhead. The received pilot signals of all time-slots $1, \dots, n$ are used for estimating x_n and $\mathbf{h}(x_n)$ in the compressed sensing and least square

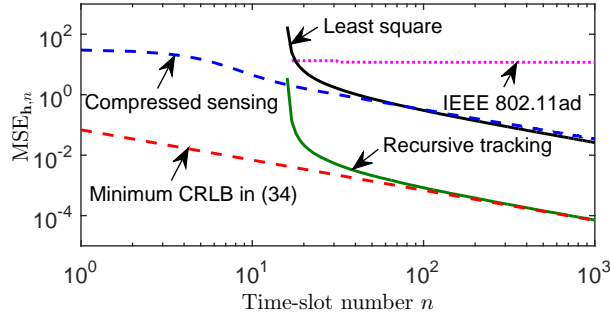


Fig. 5. $\text{MSE}_{h,n}$ vs. time-slot number n in static beam tracking.

algorithms. The step-size a_n is given by (28) with $\alpha = \alpha^*$ and $N_0 = 0$. The simulation results are averaged over 10000 random system realizations, where the beam direction x is randomly generated by a uniform distribution on $[-1, 1]$ in each realization.

Figure 5 plots the convergence performance of $\text{MSE}_{h,n}$ over time. The MSE of Algorithm 1 converges quickly to the minimum CRLB given in (34) which agrees with Corollary 1, and is much smaller than those of IEEE 802.11ad, least square and compressed sensing algorithms.

B. Dynamic Beam Tracking

In dynamic beam tracking scenarios, where beam direction changes over time, we assume that continuous pilot training is performed in the first time-slot and an initial estimate is obtained for all the algorithms. After that, one pilot is allocated in each time-slot to ensure that these algorithms have the same amount of pilot overhead.

The last $M/2$ pilot signals are used in the compressed sensing algorithm and the last M pilot signals are used in the least square algorithm. For the IEEE 802.11ad algorithm, the probing period of its beam tracking stage is 3 time-slots. These parameters are chosen to improve the performance of these algorithms. To keep track of the changing beam direction, the step-size a_n of Algorithm 1 is fixed as

$$a_n = \alpha^* = \frac{\lambda}{\sqrt{M(M-1)\pi d}}, \text{ for all } n \geq 1, \quad (42)$$

which is determined by the configuration of the antenna array and is independent of the SNR ρ .

Figures 6 and 7 depict the AoA tracking and achievable rate performance in dynamic scenarios, where the AoA θ_n varies according to $\theta_n = (\pi/3) \sin(2\pi n/1000) + 0.005\vartheta_n$ with $\vartheta_n \sim \mathcal{N}(0, 1)$. Algorithm 1 always tracks the actual AoA very well, and achieves the channel capacity 7.33bits/s/Hz in all the time-slots. The performance of Algorithm 1 is much better than the other three algorithms, and the algorithm used by IEEE 802.11ad is better than the other two.

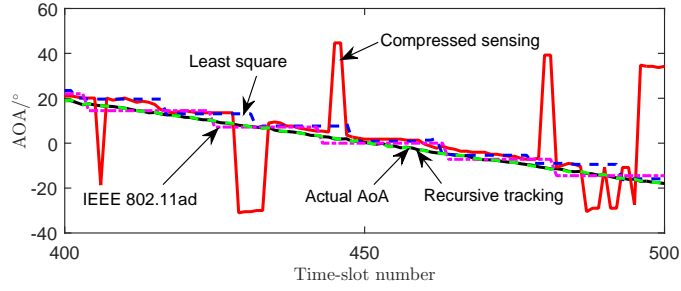


Fig. 6. AoA tracking in dynamic beam tracking.

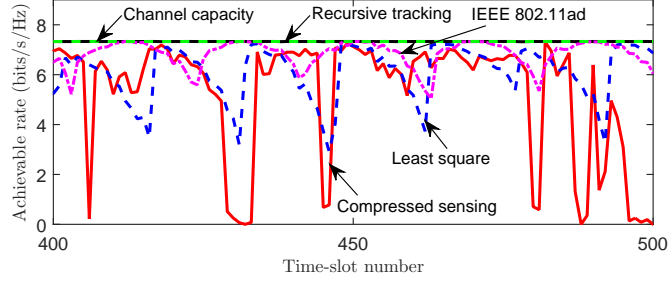


Fig. 7. Achievable rate in dynamic beam tracking.

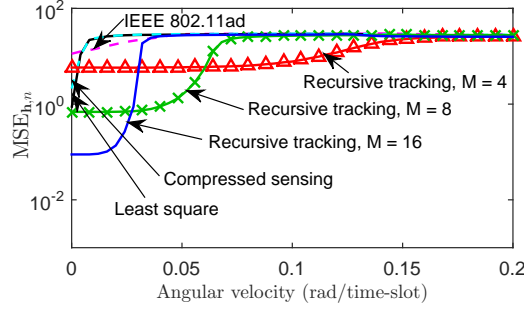


Fig. 8. $MSE_{h,n}$ vs. angular velocity in dynamic beam tracking, $\rho = 10\text{dB}$.

Figures 8 and 9 illustrate the average AoA tracking and achievable rate performance under a fixed angular velocity model $\theta_n = \theta_{n-1} + \delta_{n-1} \cdot \omega$ where $n = 1, \dots, 10000$, $\theta_0 = 0$, $\delta_n \in \{-1, 1\}$ denotes the rotation direction, and ω is a fixed angular velocity. The rotation direction δ_n is chosen such that θ_n varies within $[-\pi/3, \pi/3]$. The antenna number is 16. One can observe that Algorithm 1 can support higher angular velocities and data rates than the other algorithms when all 16 antennas are used. In addition, by using a subset of antennas, e.g., $M = 4$ or 8, for beam tracking and all 16 antennas for data transmissions, the beam tracking regime of Algorithm 1 can be further enlarged.

According to Fig. 9, Algorithm 1 can achieve 95% of the channel capacity when the angular velocity of the beam direction is 0.064rad/time-slot, the SNR is $\rho = 10\text{dB}$, and $M = 8$. If each time-slot (TTI) lasts for 0.2ms (e.g., in 5G systems [40], [41]), Algorithm 1 can support an

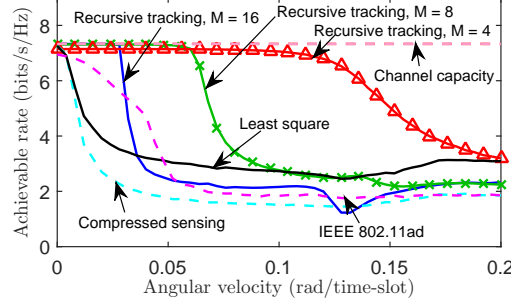


Fig. 9. Achievable rate vs. angular velocity tradeoff in dynamic beam tracking, $\rho = 10\text{dB}$.

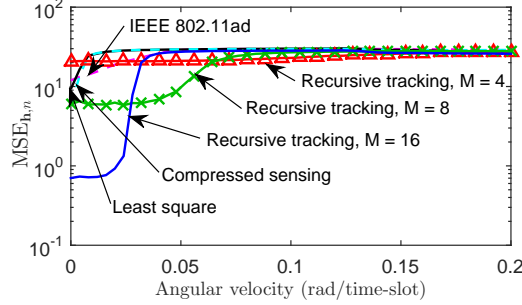


Fig. 10. $\text{MSE}_{h,n}$ vs. angular velocity in dynamic beam tracking, $\rho = 0\text{dB}$.

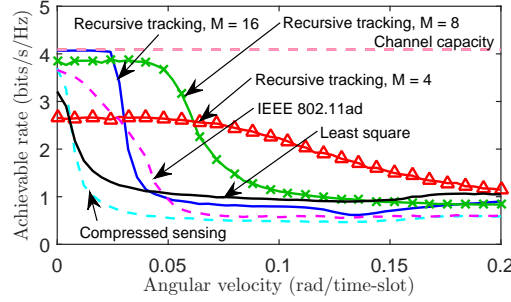


Fig. 11. Achievable rate vs. angular velocity tradeoff in dynamic beam tracking, $\rho = 0\text{dB}$.

angular velocity of $0.064 \times 1000/0.2 = 320\text{rad/s} \approx 51\text{circles/s}$. Consider a TDMA pilot pattern where 1000 narrow-beam pilots are sent to the antenna array periodically in a round-robin fashion such that 1 pilot is sent in each time-slot. Algorithm 1 can support **0.32 rad/s** (or **18.33°/s**) per beam for tracking all these 1000 beams, which is **72mph** if the transmitters/reflectors steering these beams are at a distance of 100 meters.

At last, we consider the condition that SNR is $\rho = 0\text{dB}$ and other parameters are the same as Figs. 8 and 9. As depicted in Figs. 10 and 11, it can be seen that Algorithm 1 can provide higher performance gain than the condition that SNR is $\rho = 10\text{dB}$, when all 16 antennas are used. Moreover, by using $M = 8$ antennas for tracking and all 16 antennas for data transmissions, the beam tracking regime of Algorithm 1 can still be enlarged. But when $M = 4$ antennas are used for tracking, the performance deterioration is quite significant due to the low antenna gain.

Therefore, when SNR is low, more antennas are needed to ensure the good tracking performance.

VII. CONCLUSIONS

We have developed an analog beam tracking algorithm, and established its convergence and asymptomatic optimality. Our theoretical and simulation results show that this algorithm can achieve much faster tracking speed, lower beam tracking error, and higher data rate than several state-of-the-art algorithms. In our future work, we will consider hybrid beamforming systems with multiple RF chains and two-dimensional antenna arrays, based on the methodology developed in the current paper.

REFERENCES

- [1] J. Li, Y. Sun, L. Xiao, S. Zhou, and C. E. Koksal, "Analog beam tracking in linear antenna arrays: Convergence, optimality, and performance," in *51st Asilomar Conference on Signals, Systems, and Computers*, 2017.
- [2] Z. Pi and F. Khan, "An introduction to millimeter-wave mobile broadband systems," *IEEE Commun. Mag.*, vol. 49, no. 6, Jun. 2011.
- [3] F. Boccardi, R. W. Heath, A. Lozano, T. L. Marzetta, and P. Popovski, "Five disruptive technology directions for 5G," *IEEE Commun. Mag.*, vol. 52, no. 2, Feb. 2014.
- [4] R. W. Heath, N. González-Prelcic, S. Rangan, W. Roh, and A. M. Sayeed, "An overview of signal processing techniques for millimeter wave MIMO systems," *IEEE J. Sel. Top. Signal Process.*, Apr. 2016.
- [5] T. S. Rappaport, S. Sun, R. Mayzus, H. Zhao, Y. Azar, K. Wang, G. N. Wong, J. K. Schulz, M. Samimi, and F. Gutierrez, "Millimeter wave mobile communications for 5G cellular: it will work!" *IEEE Access*, vol. 1, May 2013.
- [6] T. S. Rappaport, G. R. MacCartney, M. K. Samimi, and S. Sun, "Wideband millimeter-wave propagation measurements and channel models for future wireless communication system design," *IEEE Trans. Commun.*, vol. 63, no. 9, Sep. 2015.
- [7] T. Ohira and K. Gyoda, "Electronically steerable passive array radiator antennas for low-cost analog adaptive beamforming," in *IEEE International Conference on Phased Array Systems and Technology*, 2000.
- [8] S. Sun, T. S. Rappaport, R. W. Heath, A. Nix, and S. Rangan, "MIMO for millimeter-wave wireless communications: Beamforming, spatial multiplexing, or both?" *IEEE Commun. Mag.*, vol. 52, no. 12, Dec. 2014.
- [9] S. Han, C. L. I, Z. Xu, and C. Rowell, "Large-scale antenna systems with hybrid analog and digital beamforming for millimeter wave 5G," *IEEE Commun. Mag.*, vol. 53, no. 1, Jan. 2015.
- [10] A. Puglielli, A. Townley, G. LaCaille, V. Milovanovi, P. Lu, K. Trotskovsky, A. Whitcombe, N. Narevsky, G. Wright, T. Courtade, E. Alon, B. Nikoli, and A. M. Niknejad, "Design of energy- and cost-efficient massive MIMO arrays," *Proc. IEEE*, vol. 104, no. 3, Mar. 2016.
- [11] A. F. Molisch, V. V. Ratnam, S. Han, Z. Li, S. L. H. Nguyen, L. Li, and K. Haneda, "Hybrid beamforming for massive MIMO—a survey," *IEEE Commun. Mag.*, vol. 55, no. 9, Sep. 2017.
- [12] IEEE standard, "IEEE 802.11ad WLAN enhancements for very high throughput in the 60 GHz band," Dec. 2012.
- [13] —, "IEEE 802.15.3c WPAN millimeter-wave-based alternative physical layer extension," Oct. 2009.
- [14] METIS Report, "Final performance results and consolidated view on the most promising multi-node/multi-antenna transmission technologies," Feb. 2015.
- [15] ITU Report, "Technical feasibility of IMT in bands above 6GHz," Jul. 2015.

- [16] C. X. Wang, X. Cheng, and D. I. Laurenson, "Vehicle-to-vehicle channel modeling and measurements: recent advances and future challenges," *IEEE Commun. Mag.*, vol. 47, no. 11, Nov. 2009.
- [17] J. Wu and P. Fan, "A survey on high mobility wireless communications: Challenges, opportunities and solutions," *IEEE Access*, vol. 4, Jan. 2016.
- [18] Z. Xiao, P. Xia, and X. G. Xia, "Enabling UAV cellular with millimeter-wave communication: potentials and approaches," *IEEE Commun. Mag.*, vol. 54, no. 5, May 2016.
- [19] Keysight Technologies, "Massive MIMO and mmWave technology insight and challenges," 2015.
- [20] Samsung Electronics, "5G Vision," Feb. 2015.
- [21] A. Ghosh, "Enabling technologies for next generation wireless systems," *Nokia Bell Labs*, Mar. 2016.
- [22] W. Tong, "Bringing 5G into reality," *Huawei*, Mar. 2016.
- [23] G. Brown, O. Koymen, and M. Branda, "The promise of 5G mmWave - How do we make it mobile?" *Qualcomm Technologies*, Jun. 2016.
- [24] J. Lee, G. T. Gil, and Y. H. Lee, "Exploiting spatial sparsity for estimating channels of hybrid MIMO systems in millimeter wave communications," in *2014 IEEE GLOBECOM*, Dec. 2014.
- [25] S. Payami, M. Shariat, M. Ghorraishi, and M. Dianati, "Effective RF codebook design and channel estimation for millimeter wave communication systems," in *2015 IEEE ICC Workshop*, Jun. 2015.
- [26] D. Zhu, J. Choi, and R. W. Heath Jr, "Auxiliary beam pair enabled AoD and AoA estimation in closed-loop large-scale millimeter-wave MIMO system," *IEEE Trans. Wireless Commun.*, vol. 16, no. 7, Jul. 2017.
- [27] J. Wang, Z. Lan, C.-W. Pyo, T. Baykas, C.-S. Sum, M. A. Rahman, J. Gao, R. Funada, F. Kojima, H. Harada, and S. Kato, "Beam codebook based beamforming protocol for multi-Gbps millimeter-wave WPAN systems," *IEEE J. Sel. Areas Commun.*, vol. 27, no. 8, Oct. 2009.
- [28] S. Hur, T. Kim, D. J. Love, J. V. Krogmeier, T. A. Thomas, and A. Ghosh, "Millimeter wave beamforming for wireless backhaul and access in small cell networks," *IEEE Trans. Commun.*, Oct. 2013.
- [29] A. Alkhateeb, O. E. Ayach, G. Leus, and R. W. Heath, "Channel estimation and hybrid precoding for millimeter wave cellular systems," *IEEE J. Sel. Top. Signal Process.*, vol. 8, no. 5, Oct. 2014.
- [30] A. Alkhateeb, G. Leus, and R. W. Heath, "Limited feedback hybrid precoding for multi-user millimeter wave systems," *IEEE Trans. Wireless Commun.*, vol. 14, no. 11, Nov. 2015.
- [31] B. Gao, Z. Xiao, L. Su, Z. Chen, D. Jin, and L. Zeng, "Multi-device multi-path beamforming training for 60-GHz millimeter-wave communications," in *2015 IEEE ICC*, Jun. 2015.
- [32] A. Alkhateeb, G. Leusz, and R. W. Heath, "Compressed sensing based multi-user millimeter wave systems: How many measurements are needed?" in *IEEE ICASSP*, Apr. 2015.
- [33] R. Méndez-Rial, C. Rusu, N. González-Prelcic, A. Alkhateeb, and R. W. Heath, "Hybrid MIMO architectures for millimeter wave communications: Phase shifters or switches?" *IEEE Access*, vol. 4, Jan. 2016.
- [34] C. Zhang, D. Guo, and P. Fan, "Mobile millimeter wave channel acquisition, tracking, and abrupt change detection," *arXiv preprint arXiv:1610.09626*, 2016.
- [35] J. Palacios, D. De Donno, and J. Widmer, "Tracking mm-Wave channel dynamics: Fast beam training strategies under mobility," *IEEE INFOCOM*, 2017.
- [36] X. Gao, L. Dai, Y. Zhang, T. Xie, X. Dai, and Z. Wang, "Fast channel tracking for Terahertz beamspace massive MIMO systems," *IEEE Trans. Veh. Technol.*, vol. 66, no. 7, Jul. 2017.
- [37] N. Garcia, H. Wymeersch, and D. Slock, "Optimal robust precoders for tracking the AoD and AoA of a mm-Wave path," *arXiv preprint arXiv:1703.10978*, 2017.

- [38] J. Bae, S. H. Lim, J. H. Yoo, and J. W. Choi, “New beam tracking technique for millimeter wave-band communications,” *arXiv preprint arXiv:1702.00276*, 2017.
- [39] E. Karami, “Tracking performance of least squares MIMO channel estimation algorithm,” *IEEE Trans. Commun.*, vol. 55, no. 11, Nov. 2007.
- [40] K. I. Pedersen, G. Berardinelli, F. Frederiksen, P. Mogensen, and A. Szufarska, “A flexible 5G frame structure design for frequency-division duplex cases,” *IEEE Commun. Mag.*, vol. 54, no. 3, Mar. 2016.
- [41] P. Zong, “5G and the path to 5G,” *Intel Corporation*, Oct. 2016.
- [42] M. B. Nevel’son and R. Z. Has’minskii, *Stochastic approximation and recursive estimation*, 1973.
- [43] H. V. Poor, *An introduction to signal detection and estimation*. New York, NY, USA: Springer-Verlag New York, Inc., 1994.
- [44] V. S. Borkar, *Stochastic approximation: a dynamical systems viewpoint*, 2008.
- [45] H. Kushner and G. G. Yin, *Stochastic approximation and recursive algorithms and applications*. Springer Science & Business Media, 2003, vol. 35.
- [46] G. Yin and K. Yin, “Asymptotically optimal rate of convergence of smoothed stochastic recursive algorithms,” *Stochastics and Stochastic Reports*, vol. 47, 1994.
- [47] J. M. Holte, “Discrete Gronwall lemma and applications,” in *MAA-NCS meeting at the University of North Dakota*, vol. 24, 2009.
- [48] W. Hoeffding, “Probability inequalities for sums of bounded random variables,” *J. Am. Stat. Assoc.*, vol. 58, no. 301, 1963.

APPENDIX A

PROOF OF THEOREM 1

Before providing the proof, let us define some useful variables first. Recall the recursive procedure (15) and (16):

$$\hat{x}_n = [\hat{x}_{n-1} - a_n \operatorname{Im} \{y_n\}]_{-1}^1,$$

where

$$-\operatorname{Im} \{y_n\} = f(\hat{x}_{n-1}, x) + \hat{z}_n, \tag{43}$$

$f(\hat{x}_{n-1}, x)$ is defined in (25), and

$$\hat{z}_n \triangleq -\frac{\operatorname{Im} \{z_n\}}{\sqrt{\rho}} \sim \mathcal{N}\left(0, \frac{1}{2\rho}\right). \tag{44}$$

Let $\{\mathcal{G}_n : n \geq n_0\}$ be an increasing sequence of σ -fields of $\{\hat{x}_{n_0}, \hat{z}_{n_0+1}, \hat{z}_{n_0+2}, \dots\}$, i.e., $\mathcal{G}_{n-1} \subset \mathcal{G}_n$, where $\mathcal{G}_{n_0} \triangleq \sigma(\hat{x}_{n_0})$ and $\mathcal{G}_n \triangleq \sigma(\hat{x}_{n_0}, \hat{z}_{n_0+1}, \dots, \hat{z}_n)$ for $n \geq n_0 + 1$. Because the \hat{z}_n ’s are *i.i.d.* circularly symmetric complex Gaussian random variables with zero mean, \hat{z}_n is independent

of \mathcal{G}_{n-1} , and $\hat{x}_{n-1} \in \mathcal{G}_{n-1}$. Hence, we have

$$\begin{aligned}
\mathbb{E}[-\operatorname{Im}\{y_n\}|\mathcal{G}_{n-1}] &= \mathbb{E}[f(\hat{x}_{n-1}, x) + \hat{z}_n|\mathcal{G}_{n-1}] \\
&= \mathbb{E}[f(\hat{x}_{n-1}, x)|\mathcal{G}_{n-1}] + \mathbb{E}[\hat{z}_n|\mathcal{G}_{n-1}] \\
&= f(\hat{x}_{n-1}, x),
\end{aligned} \tag{45}$$

for $n \geq n_0 + 1$.

Theorem 5.2.1 in [45, Section 5.2.1] provided the sufficient conditions under which \hat{x}_n converges to a unique point within a set of stable points with probability one. We will prove that when the step-size a_n is given by (28) with any $\alpha > 0$ and $N_0 \geq 0$, our algorithm satisfies its sufficient conditions below:

1) Step-size requirements:

$$\begin{aligned}
a_n &= \frac{\alpha}{n - n_0 + N_0} \rightarrow 0, \\
\sum_{n=n_0+1}^{\infty} a_n &= \sum_{n=n_0+1}^{\infty} \frac{\alpha}{n - n_0 + N_0} = \sum_{i=1}^{\infty} \frac{\alpha}{i + N_0} = \infty, \\
\sum_{n=n_0+1}^{\infty} a_n^2 &= \sum_{n=n_0+1}^{\infty} \frac{\alpha^2}{(n - n_0 + N_0)^2} \\
&\leq \sum_{n=n_0+1}^{\infty} \frac{\alpha^2}{(n - n_0)^2} = \sum_{i=1}^{\infty} \frac{\alpha^2}{i^2} < \infty.
\end{aligned}$$

2) We need to prove that $\sup_n \mathbb{E}[|-\operatorname{Im}\{y_n\}|^2] < \infty$.

From (43), we have

$$\begin{aligned}
&\mathbb{E}[|-\operatorname{Im}\{y_n\}|^2] \\
&\stackrel{(a)}{=} \mathbb{E}[|f(\hat{x}_{n-1}, x)|^2 + 2f(\hat{x}_{n-1}, x)\hat{z}_n + \hat{z}_n^2] \\
&\stackrel{(b)}{=} \mathbb{E}[|f(\hat{x}_{n-1}, x)|^2] + \frac{1}{2\rho},
\end{aligned} \tag{46}$$

where step (a) is due to (43) and step (b) is due to that \hat{z}_n defined in (44) is independent of $f(\hat{x}_{n-1}, x)$.

From (25), we have

$$\begin{aligned} |f(\hat{x}_{n-1}, x)| &\leq \left| \frac{1}{\sqrt{M}} \sum_{m=1}^M e^{j \frac{2\pi d}{\lambda} (m-1)(\hat{x}_{n-1}-x)} \right| \\ &\leq \frac{1}{\sqrt{M}} \sum_{m=1}^M \left| e^{j \frac{2\pi d}{\lambda} (m-1)(\hat{x}_{n-1}-x)} \right| \leq \sqrt{M}, \end{aligned} \quad (47)$$

so we get

$$\mathbb{E} [|f(\hat{x}_{n-1}, x)|^2] \leq M < \infty. \quad (48)$$

Combining (46) and (48), we have

$$\sup_n \mathbb{E} [|- \operatorname{Im} \{y_n\}|^2] < \infty.$$

- 3) The function $f(v, x)$ should be continuous with respect to v .

From (25), $f(v, x)$ can be rewritten as follows:

$$f(v, x) = -\frac{1}{\sqrt{M}} \sum_{m=1}^M \sin \left[\frac{2\pi d}{\lambda} (m-1)(v-x) \right].$$

Because $\sin \left[\frac{2\pi d}{\lambda} (m-1)(v-x) \right]$ is continuous with respect to v , and $f(v, x)$ is the summation of a finite amount of $\sin \left[\frac{2\pi d}{\lambda} (m-1)(v-x) \right]$, $m = 1, \dots, M$. Therefore, we can conclude that $f(v, x)$ is continuous with respect to v .

- 4) Let $\gamma_n = \mathbb{E} [-\operatorname{Im} \{y_n\} | \mathcal{G}_{n-1}] - f(\hat{x}_{n-1}, x)$. We need to prove that $\sum_{n=n_0+1}^{\infty} |a_n \gamma_n| < \infty$ with probability one.

From (45), we get $\gamma_n = 0$ for all $n \geq n_0 + 1$. So we have $\sum_{n=n_0+1}^{\infty} |a_n \gamma_n| = 0 < \infty$ with probability one.

- 5) The set of stable points for the ODE (26) should be obtained.

According to (27), $\mathcal{S}(x)$ contains the local optimal stable points for the ODE (26). What's more, the boundary point 1 (or -1) is a stable point when $f(1, x) \geq 0$ (or $f(-1, x) \leq 0$).

Hence, the set of stable points is a subset of $\mathcal{S}(x) \cup \{-1\} \cup \{1\}$.

By Theorem 5.2.1 in [45], \hat{x}_n converges to a unique point within $\mathcal{S}(x) \cup \{-1\} \cup \{1\}$ with probability one.

APPENDIX B

PROOF OF THEOREM 2

Theorem 2 is proven in three steps:

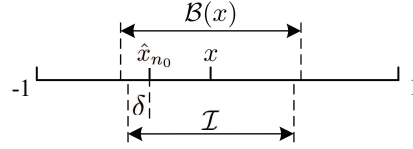


Fig. 12. An illustration of the invariant set \mathcal{I} .

Step 1: We will construct two continuous processes, i.e., $\bar{x}(t)$ and $\tilde{x}^n(t)$, based on the discrete process $\{\hat{x}_n\}$.

We first define the discrete time parameters: $t_{n_0} \triangleq 0$, $t_n \triangleq \sum_{i=n_0+1}^n a_i$, $n \geq n_0 + 1$.

The first continuous process $\bar{x}(t)$, $t \geq 0$ is the linear interpolation of the sequence $\{\hat{x}_n : n \geq n_0\}$, where $\bar{x}(t_n) = \hat{x}_n$, $n \geq n_0$ and $\bar{x}(t)$ is given by

$$\bar{x}(t) = \bar{x}(t_n) + \frac{(t - t_n) [\bar{x}(t_{n+1}) - \bar{x}(t_n)]}{a_{n+1}}, t \in [t_n, t_{n+1}]. \quad (49)$$

The second continuous process $\tilde{x}^n(t)$ is a solution of the ODE (26) for $t \in [t_n, \infty)$, where $\tilde{x}^n(t_n) = \bar{x}(t_n) = \hat{x}_n$, $n \geq n_0$. Since we only care about the condition that $\hat{x}_n \in \mathcal{B}(x)$, there exist two cases: (i) if $\pm 1 \notin \mathcal{B}(x)$, then the solution of the ODE (26) is within $(-1, 1)$, (ii) if 1 (or -1) is in $\mathcal{B}(x)$, then $f(1, x) \leq 0$ (or $f(-1, x) \geq 0$)⁶. Hence, the projection operation in the ODE (26) will not take effect and we can omit it. Then, we have $\frac{d\tilde{x}^n(t)}{dt} = f(\tilde{x}^n(t), x)$ and

$$\tilde{x}^n(t) = \bar{x}(t_n) + \int_{t_n}^t f(\tilde{x}^n(v), x) dv, t \geq t_n. \quad (50)$$

Step 2: By using the continuous processes $\bar{x}(t)$ and $\tilde{x}^n(t)$, we will form a sufficient condition for the convergence of the discrete process $\{\hat{x}_n\}$.

We first construct a time-invariant set \mathcal{I} that contains the real direction x within the mainlobe, i.e., $x \in \mathcal{I} \subset \mathcal{B}(x)$. Pick δ such that⁷

$$\inf_{v \in \partial \mathcal{B}(x)} |v - \hat{x}_{n_0}| > \delta > 0.$$

Then, the invariant set \mathcal{I} can be constructed as follows:

$$\mathcal{I} = \left(x - |x - \hat{x}_{n_0}| - \delta, x + |x - \hat{x}_{n_0}| + \delta \right) \subset \mathcal{B}(x). \quad (51)$$

An example of the invariant set \mathcal{I} is illustrated in Fig. 12.

⁶This property can be verified by shifting the curves in Fig. 3.

⁷The boundary of the set $\mathcal{B}(x)$ is denoted by $\partial \mathcal{B}(x)$.

Then, we will establish a sufficient condition in Lemma 1 that ensures $\hat{x}_n \in \mathcal{I}$ for $n \geq n_0$, and hence from Corollary 2.5 in [44], we can obtain that $\{\hat{x}_n\}$ converges to x . Before giving Lemma 1, let us provide some definitions first:

- Pick $T > 0$ such that the solution $x(t), t \geq 0$ of the ODE (26) with $x(0) = \hat{x}_{n_0}$ satisfies $\inf_{v \in \partial \mathcal{I}} |v - x(t)| > 2\delta$ for $t \geq T$. Since the solution $x(t)$ of the ODE (26) will approach the real direction x monotonically within the mainlobe $\mathcal{B}(x)$ as time t increases, we have $|\hat{x}_{n_0} - x(T)| > \delta$ and one possible value of T is given by

$$T = \max \left\{ \frac{\delta}{|f(\hat{x}_{n_0}, x)|}, \frac{\delta}{|f(|\hat{x}_{n_0} - x| - \delta + x, x)|} \right\}. \quad (52)$$

- Let $T_0 \triangleq 0$ and $T_{m+1} \triangleq \min \{t_i : t_i \geq T_n + T, i \geq n_0\}$ for $m \geq 0$. Then $T_{m+1} - T_m \in [T, T + a_{n_0}]$ and $T_m = t_{\tilde{n}(m)}$ for some $\tilde{n}(m) \uparrow \infty$, where $\tilde{n}(0) = n_0$. Let $\tilde{x}^{\tilde{n}(m)}(t)$ denote the solution of ODE (26) for $t \in I_m \triangleq [T_m, T_{m+1}]$ with $\tilde{x}^{\tilde{n}(m)}(T_m) = \bar{x}(T_m)$, $m \geq 0$.

Hence, we can obtain the following lemma:

Lemma 1. If $\sup_{t \in I_m} |\bar{x}(t) - \tilde{x}^{\tilde{n}(m)}(t)| \leq \delta$ for all $m \geq 0$, then $\hat{x}_n \in \mathcal{I}$ for all $n \geq n_0$.

Proof. See Appendix E □

Step 3: We will derive the probability lower bound for the condition in Lemma 1, which is also a lower bound for $P(\hat{x}_n \rightarrow x | \hat{x}_{n_0} \in \mathcal{B}(x))$.

We will derive the probability lower bound for the condition in Lemma 1, which results in the following lemma:

Lemma 2. If (i) the initial point satisfies $\hat{x}_{n_0} \in \mathcal{B}(x)$, (ii) a_n is given by (28) with any $\alpha > 0$, then there exist $N_0 \geq 0$ and $C(\hat{x}_{n_0}) > 0$ such that

$$\begin{aligned} & P(\hat{x}_n \in \mathcal{I}, \forall n \geq n_0) \\ & \geq P\left(\sup_{t \in I_m} |\bar{x}(t) - \tilde{x}^{\tilde{n}(m)}(t)| \leq \delta, \forall m \geq 0\right) \\ & \geq 1 - 2e^{-C(\hat{x}_{n_0}) \cdot \frac{\rho}{\alpha^2}}. \end{aligned} \quad (53)$$

Proof. See Appendix F. □

Finally, by applying Lemma 2 and Corollary 2.5 in [44], we can obtain

$$\begin{aligned} P(\hat{x}_n \rightarrow x | \hat{x}_{n_0} \in \mathcal{B}) &\geq P(\hat{x}_n \in \mathcal{I}, \forall n \geq n_0) \\ &\geq 1 - 2e^{-C(\hat{x}_{n_0}) \cdot \frac{\rho}{\alpha^2}}, \end{aligned} \quad (54)$$

which completes the proof of Theorem 2.

APPENDIX C

PROOF OF THEOREM 3

When the step-size a_n is given by (28) with any $\alpha > 0$ and $N_0 \geq 0$, Theorem 6.6.1 [42, Section 6.6] has proposed the sufficient conditions to prove the asymptotic normality of $\sqrt{n - n_0 + N_0}(\hat{x}_n - x)$, i.e., $\sqrt{n - n_0 + N_0}(\hat{x}_n - x) \xrightarrow{d} \mathcal{N}(0, \Sigma)$. Under the condition that $\hat{x}_n \rightarrow x$, we will prove that our algorithm satisfies its sufficient conditions and obtain the variance Σ as follows:

- 1) The estimate \hat{x}_n should be within $[-1, 1]$.

The projection operator in (16) ensures that $\hat{x}_n \in [-1, 1]$.

- 1) Equation (43) should satisfy: (i) there exist an increasing sequence of σ -fields $\{\mathcal{F}_n : n \geq n_0\}$ such that $\mathcal{F}_m \subset \mathcal{F}_n$ for $m < n$, and (ii) the random noise \hat{z}_n is \mathcal{F}_n -measurable and independent of \mathcal{F}_{n-1} .

As defined in Appendix A, there exist an increasing sequence of σ -fields $\{\mathcal{G}_n : n \geq n_0\}$, such that \hat{z}_n is measurable with respect to \mathcal{G}_n , i.e., $\mathbb{E}[\hat{z}_n | \mathcal{G}_n] = \hat{z}_n$, and is independent of \mathcal{G}_{n-1} , i.e., $\mathbb{E}[\hat{z}_n | \mathcal{G}_{n-1}] = \mathbb{E}[\hat{z}_n] = 0$.

- 2) \hat{x}_n should converge to x almost surely as $n \rightarrow \infty$.

Since $\hat{x}_n \rightarrow x$ is assumed, we have that \hat{x}_n converges to x almost surely as $n \rightarrow \infty$.

- 3) The stable condition:

From (25), $f(v, x)$ can be rewritten as follows:

$$\begin{aligned} f(v, x) &= - \frac{\sin \left[\frac{(M-1)\pi d}{\lambda} (v - x) \right] \sin \left[\frac{M\pi d}{\lambda} (v - x) \right]}{\sqrt{M} \sin \left[\frac{\pi d}{\lambda} (v - x) \right]} \\ &= - \frac{1}{\sqrt{M}} c_1 (v - x) + o(v - x), \end{aligned}$$

where c_1 is given by

$$c_1 = \left\{ \frac{\sin \left[\frac{(M-1)\pi d}{\lambda} (v-x) \right] \sin \left[\frac{M\pi d}{\lambda} (v-x) \right]}{\sin \left[\frac{\pi d}{\lambda} (v-x) \right]} \right\}'_{v=x} \\ = \frac{M(M-1)\pi d}{\lambda}.$$

Then we get the stable condition that

$$A = -\frac{c_1}{\sqrt{M}} \cdot \alpha + \frac{1}{2} = -\frac{\sqrt{M}(M-1)\pi d \alpha}{\lambda} + \frac{1}{2} < 0,$$

which results in $\alpha > \frac{\lambda}{2\sqrt{M}(M-1)\pi d}$.

4) The constraints for the random noise:

$$\mathbb{E} [(\hat{z}_n)^2] = \frac{1}{2\rho} < \infty,$$

and

$$\lim_{V \rightarrow \infty} \sup_{n \geq 1} \int_{|\hat{z}_n| > V} |\hat{z}_n|^2 p(\hat{z}_n) d\hat{z}_n = 0.$$

Hence, we have

$$\sqrt{n - n_0 + N_0} (\hat{x}_n - x) \xrightarrow{d} \mathcal{N}(0, \Sigma),$$

where

$$\Sigma = \alpha^2 \mathbb{E} [(\hat{z}_n)^2] \cdot \int_0^\infty e^{2Av} dv \\ = \frac{\alpha^2}{2\rho \left(\frac{2\sqrt{M}(M-1)\pi d \alpha}{\lambda} - 1 \right)}. \quad (55)$$

Due to that $\lim_{n \rightarrow \infty} \sqrt{(n - n_0 + N_0)/n} = 1$, we have

$$\sqrt{n} (\hat{x}_n - x) \rightarrow \sqrt{n} \cdot \sqrt{\frac{n - n_0 + N_0}{n}} (\hat{x}_n - x) \xrightarrow{d} \mathcal{N}(0, \Sigma),$$

as $n \rightarrow \infty$. By adapting α in (55), we can obtain different Σ , which achieves the minimum value $\Sigma_{\min} = I_{\max}^{-1}$, i.e., the minimum CRLB in (12), when $\alpha = \frac{\lambda}{\sqrt{M}(M-1)\pi d}$.

By assuming $\alpha = \frac{\lambda}{\sqrt{M}(M-1)\pi d}$, we conclude that

$$\lim_{n \rightarrow \infty} n \mathbb{E} [(\hat{x}_n - x)^2 | \hat{x}_n \rightarrow x] = I_{\max}^{-1}.$$

APPENDIX D
PROOF OF COROLLARY 1

Let $\mathbf{u}(x) = [u_1(x), \dots, u_N(x)]^T$ be a N -dimensional vector function, which is first-order differentiable. Similar to (8)-(12), its MSE is lower bounded by

$$\begin{aligned} \mathbb{E} [\|\mathbf{u}(\hat{x}_n) - \mathbf{u}(x)\|_2^2] &= \sum_{m=1}^N \mathbb{E} [(u_m(\hat{x}_n) - u_m(x))^2] \\ &\geq \sum_{m=1}^N \frac{1}{nI'_{\max,m}}, \end{aligned} \quad (56)$$

where $I'_{\max,i}$ is given by

$$I'_{\max,m} = \mathbb{E} \left[\left(\frac{\partial \log p(y_i|x, \mathbf{w}_i)}{\partial u_m(x)} \right)^2 \middle| x, \mathbf{w}_i = \frac{\mathbf{a}(x)}{\sqrt{M}} \right].$$

According to Theorem 3, we have

$$\lim_{n \rightarrow \infty} n \mathbb{E} [(\hat{x}_n - x)^2 | \hat{x}_n \rightarrow x] = I_{\max}^{-1},$$

where I_{\max} is given by

$$\begin{aligned} I_{\max} &= \mathbb{E} \left[-\frac{\partial^2 \log p(y_i|x, \mathbf{w}_i)}{\partial x^2} \middle| x, \mathbf{w}_i = \frac{\mathbf{a}(x)}{\sqrt{M}} \right] \\ &= \mathbb{E} \left[\left(\frac{\partial \log p(y_i|x, \mathbf{w}_i)}{\partial x} \right)^2 \middle| x, \mathbf{w}_i = \frac{\mathbf{a}(x)}{\sqrt{M}} \right]. \end{aligned}$$

Since $\frac{\partial \log p(y_i|x, \mathbf{w}_i)}{\partial x}$ can be rewritten as

$$\frac{\partial \log p(y_i|x, \mathbf{w}_i)}{\partial x} = \frac{\partial \log p(y_i|x, \mathbf{w}_i)}{\partial u_m(x)} \cdot u'_m(x),$$

we get

$$I'_{\max,m} = \frac{I_{\max}}{[u'_m(x)]^2},$$

which results in

$$\lim_{n \rightarrow \infty} n \mathbb{E} [|u_m(\hat{x}_n) - u_m(x)|^2 | \hat{x}_n \rightarrow x] = [u'_m(x)]^2 I_{\max}^{-1}.$$

Then, based on (56), we conclude that

$$\lim_{n \rightarrow \infty} n \mathbb{E} \left[\|\mathbf{u}(\hat{x}_n) - \mathbf{u}(x)\|_2^2 \middle| \hat{x}_n \rightarrow x \right] = \|\mathbf{u}'(x)\|_2^2 I_{\max}^{-1}.$$

APPENDIX E

PROOF OF LEMMA 1

When $m = 0$, $\tilde{x}^{\tilde{n}(0)}(T_0) = \bar{x}(T_0) = \hat{x}_{n_0}$. There are two symmetrical cases: (i) $\hat{x}_{n_0} < x$ and (ii) $\hat{x}_{n_0} > x$. We will consider the *first case*, which can be directly extended to the *second case*.

Case 1 ($\hat{x}_{n_0} < x$): We will first prove that $\bar{x}(t) \in \mathcal{I} = \left(x - |x - \hat{x}_{n_0}| - \delta, x + |x - \hat{x}_{n_0}| + \delta \right)$ for all $t \in I_0$.

If $|\bar{x}(t) - \tilde{x}^{\tilde{n}(0)}(t)| \leq \delta$ for all $t \in I_0$, then we have $\bar{x}(t) - \tilde{x}^{\tilde{n}(0)}(t) \geq -\delta$. What's more, due to $\hat{x}_{n_0} \in \mathcal{I} \subset \mathcal{B}(x)$ and the monotonic property of the ODE (26) within the mainlobe $\mathcal{B}(x)$, we get $\tilde{x}^{\tilde{n}(0)}(t) - \hat{x}_{n_0} \geq 0$ and $x - \tilde{x}^{\tilde{n}(0)}(t) \geq 0$ for all $t \in I_0$. Therefore, we can obtain

$$\begin{aligned} & \bar{x}(t) - (\hat{x}_{n_0} - \delta) \\ &= [\bar{x}(t) - \tilde{x}^{\tilde{n}(0)}(t)] + [\tilde{x}^{\tilde{n}(0)}(t) - \hat{x}_{n_0}] + \delta \geq 0, \end{aligned} \tag{57}$$

and

$$\begin{aligned} & (x + |x - \hat{x}_{n_0}| + \delta) - \bar{x}(t) \\ &= (2x - \hat{x}_{n_0} + \delta) - \bar{x}(t) \\ &= (x - \hat{x}_{n_0}) + [x - \bar{x}(t)] + \delta \\ &= (x - \hat{x}_{n_0}) + [x - \tilde{x}^{\tilde{n}(0)}(t)] + [\tilde{x}^{\tilde{n}(0)}(t) - \bar{x}(t)] + \delta \\ &\geq 0, \end{aligned} \tag{58}$$

which result in $\bar{x}(t) \in \mathcal{I}$ for all $t \in I_0$.

Then, we consider the initial value $\bar{x}(T_1)$ for the next time interval I_1 . With the T given by (52), we have

$$x - \hat{x}_{n_0} \geq \tilde{x}^{\tilde{n}(0)}(T_1) - \hat{x}_{n_0} \geq \tilde{x}^{\tilde{n}(0)}(T) - \hat{x}_{n_0} > \delta.$$

Therefore, we get

$$\begin{aligned} & \bar{x}(T_1) - \hat{x}_{n_0} \\ &= [\bar{x}(T_1) - \tilde{x}^{\tilde{n}(0)}(T_1)] + [\tilde{x}^{\tilde{n}(0)}(T_1) - \hat{x}_{n_0}] \geq 0, \end{aligned} \tag{59}$$

and

$$\begin{aligned} & (x + |x - \hat{x}_{n_0}|) - \bar{x}(T_1) \\ &= (2x - \hat{x}_{n_0}) - \bar{x}(T_1) \\ &= (x - \hat{x}_{n_0}) + [x - \bar{x}(T_1)] \\ &= (x - \hat{x}_{n_0}) + [x - \tilde{x}^{\tilde{n}(0)}(T_1)] + [\tilde{x}^{\tilde{n}(0)}(T_1) - \bar{x}(T_1)] \\ &\geq 0, \end{aligned} \tag{60}$$

which result in $\bar{x}(T_1) \in [x - |x - \hat{x}_{n_0}|, x + |x - \hat{x}_{n_0}|]$.

Case 2 ($\hat{x}_{n_0} > x$): Owing to symmetric property, we can use the same method as (57)-(60) to obtain that $\bar{x}(t) \in \mathcal{I}$ for all $t \in I_0$ and $\bar{x}(T_1) \in [x - |x - \hat{x}_{n_0}|, x + |x - \hat{x}_{n_0}|]$.

When $m = 1$, $\tilde{x}^{\tilde{n}(1)}(T_1) = \bar{x}(T_1) \in [x - |x - \hat{x}_{n_0}|, x + |x - \hat{x}_{n_0}|]$. If $\bar{x}(T_1) < x$ and $|\bar{x}(t) - \tilde{x}^{\tilde{n}(1)}(t)| \leq \delta$, then for all $t \in I_1$, we have $\bar{x}(T_1) \geq \hat{x}_{n_0}$, $\tilde{x}^{\tilde{n}(1)}(t) - \hat{x}_{n_0} \geq 0$, $x - \tilde{x}^{\tilde{n}(1)}(t) \geq 0$, and

$$x - \hat{x}_{n_0} \geq \tilde{x}^{\tilde{n}(1)}(T_2) - \hat{x}_{n_0} \geq \tilde{x}^{\tilde{n}(1)}(T_1 + T) - \hat{x}_{n_0} > \delta.$$

Similar to (57)-(60), we can get $\bar{x}(t) \in \mathcal{I}$ for all $t \in I_1$ and $\bar{x}(T_2) \in [x - |x - \hat{x}_{n_0}|, x + |x - \hat{x}_{n_0}|]$, which are also true for the case that $\bar{x}(T_1) > x$.

Hence, we can use the same method to prove the case of $m \geq 2$, which finally yields $\bar{x}(t) \in \mathcal{I}$ for all $t \in I_m$ and $m \geq 0$. Since $\bar{x}(t_n) = \hat{x}_n$ for all $n \geq n_0$, we can obtain that $\hat{x}_n \in \mathcal{I}$ for all $n \geq n_0$, which completes the proof.

APPENDIX F

PROOF OF LEMMA 2

The following lemmas are needed to prove Lemma 2:

Lemma 3. Given n_T by (65), if there exists a constant $C > 0$, which satisfies

$$\begin{aligned} & |\bar{x}(t_{n+m}) - \tilde{x}^n(t_{n+m})| \\ & \leq L \sum_{i=1}^m a_{n+i} |\bar{x}(t_{n+i-1}) - \tilde{x}^n(t_{n+i-1})| + C, \end{aligned} \quad (61)$$

for all $n \geq n_0$ and $1 \leq m \leq n_T$, then

$$\sup_{t \in [t_n, t_{n+n_T}]} |\bar{x}(t) - \tilde{x}^n(t)| \leq \frac{\sqrt{M}a_{n+1}}{2} + Ce^{L(T+a_{n_0})}. \quad (62)$$

Proof. See Appendix G. □

Lemma 4. If $\{M_i : i = 1, 2, \dots\}$ is a Gaussian martingale, then

$$P \left(\sup_{0 \leq i \leq k} |M_i| > \eta \right) \leq 2 \exp \left\{ -\frac{\eta^2}{2 \text{Var}[M_k]} \right\}, \quad (63)$$

for any $\eta > 0$.

Proof. See Appendix H. □

Lemma 5. If given a constant $C > 0$, then

$$G(v) = \frac{1}{v} \exp \left[-\frac{C}{v} \right], \quad (64)$$

is increasing for all $0 < v < C$.

Proof. The derivative of $G(v)$ is

$$G'(v) = \frac{C-v}{v^3} \exp \left[-\frac{C}{v} \right].$$

Let $G'(v) > 0$ and we can obtain that $G(v)$ is increasing for $v \in (0, C)$, which completes the proof. □

Let $\xi_{n_0} \triangleq 0$ and $\xi_n \triangleq \sum_{m=n_0+1}^n a_m \hat{z}_m$, $n \geq n_0 + 1$, where \hat{z}_m is defined in (44). Given T by (52), we define

$$n_T \triangleq \inf \{i \in \mathbb{Z} : t_{n+i} \geq t_n + T\}. \quad (65)$$

With (49) and (50), we have for t_{n+m} , $1 \leq m \leq n_T$,

$$\bar{x}(t_{n+m}) = \bar{x}(t_n) + \sum_{i=1}^m a_{n+i} f(\bar{x}(t_{n+i-1}), x) + (\xi_{n+m} - \xi_n), \quad (66)$$

and

$$\begin{aligned} \tilde{x}^n(t_{n+m}) &= \tilde{x}^n(t_n) + \int_{t_n}^{t_{n+m}} f(\tilde{x}^n(v), x) dv \\ &= \tilde{x}^n(t_n) + \sum_{i=1}^m a_{n+i} f(\tilde{x}^n(t_{n+i-1}), x) + \int_{t_n}^{t_{n+m}} [f(\tilde{x}^n(v), x) - f(\tilde{x}^n(\underline{v}), x)] dv, \end{aligned} \quad (67)$$

where $\underline{v} \triangleq \max \{t_n : t_n \leq v, n \geq n_0\}$ for $v \geq 0$.

To bound $\int_{t_n}^{t_{n+m}} [f(\tilde{x}^n(v), x) - f(\tilde{x}^n(\underline{v}), x)] dv$ on the RHS of (67), we obtain the Lipschitz constant of function $f(v, x)$ considering the first variable v , given by

$$L \triangleq \sup_{v_1 \neq v_2} \frac{|f(v_1, x) - f(v_2, x)|}{|v_1 - v_2|}. \quad (68)$$

Plugging (25) into (68), yields $L = \frac{\sqrt{M(M-1)}\pi d}{\lambda}$, which is not related to x . Similar to (47), for any $t \geq t_n$, we can obtain

$$|f(\tilde{x}^n(t), x)| \leq \sqrt{M}. \quad (69)$$

Hence, we have

$$\begin{aligned}
& \left| \int_{t_n}^{t_{n+m}} [f(\tilde{x}^n(v), x) - f(\tilde{x}^n(\underline{v}), x)] dv \right| \\
& \leq \int_{t_n}^{t_{n+m}} |f(\tilde{x}^n(v), x) - f(\tilde{x}^n(\underline{v}), x)| dv \\
& \stackrel{(a)}{\leq} \int_{t_n}^{t_{n+m}} L |\tilde{x}^n(v) - \tilde{x}^n(\underline{v})| dv \\
& \stackrel{(b)}{\leq} \int_{t_n}^{t_{n+m}} L \left| \int_{\underline{v}}^v f(\tilde{x}^n(s), x) ds \right| dv \\
& \leq \int_{t_n}^{t_{n+m}} \int_{\underline{v}}^v L |f(\tilde{x}^n(s), x)| ds dv \\
& \stackrel{(c)}{\leq} \int_{t_n}^{t_{n+m}} \int_{\underline{v}}^v \sqrt{M} L ds dv = \int_{t_n}^{t_{n+m}} \sqrt{M} L (v - \underline{v}) dv \\
& = \sum_{i=1}^m \int_{t_{n+i-1}}^{t_{n+i}} \sqrt{M} L (v - t_{n+i-1}) dv \\
& = \sum_{i=1}^m \frac{\sqrt{M} L (t_{n+i} - t_{n+i-1})^2}{2} = \frac{\sqrt{M} L}{2} \sum_{i=1}^m a_{n+i}^2,
\end{aligned} \tag{70}$$

where step (a) is due to (68), step (b) is due to the definition in (50), and step (c) is due to (69). Then, by subtracting $\tilde{x}^n(t_{n+m})$ in (67) from $\bar{x}(t_{n+m})$ in (66) and taking norms, the following inequality can be obtained from (68) and (70) for $n \geq n_0$:

$$\begin{aligned}
& |\bar{x}(t_{n+m}) - \tilde{x}^n(t_{n+m})| \\
& \leq L \sum_{i=1}^m a_{n+i} |\bar{x}(t_{n+i-1}) - \tilde{x}^n(t_{n+i-1})| + \frac{\sqrt{M} L}{2} \sum_{i=1}^m a_{n+i}^2 + |\xi_{n+m} - \xi_n| \\
& \leq L \sum_{i=1}^m a_{n+i} |\bar{x}(t_{n+i-1}) - \tilde{x}^n(t_{n+i-1})| + \frac{\sqrt{M} L}{2} \sum_{i=1}^{n_T} a_{n+i}^2 + \sup_{1 \leq m \leq n_T} |\xi_{n+m} - \xi_n|.
\end{aligned} \tag{71}$$

Applying Lemma 3 to (71) and letting

$$C = \frac{\sqrt{M} L}{2} \sum_{i=1}^{n_T} a_{n+i}^2 + \sup_{1 \leq m \leq n_T} |\xi_{n+m} - \xi_n|,$$

yields

$$\begin{aligned}
& \sup_{t \in [t_n, t_{n+n_T}]} |\bar{x}(t) - \tilde{x}^n(t)| \\
& \leq C_e \left\{ \frac{\sqrt{M} L}{2} [b(n) - b(n + n_T)] + \sup_{1 \leq m \leq n_T} |\xi_{n+m} - \xi_n| \right\} + \frac{\sqrt{M} a_{n+1}}{2},
\end{aligned} \tag{72}$$

where $C_e \triangleq e^{L(T+a_{n_0})}$, and $b(n) \triangleq \sum_{i>n} a_i^2$. Letting $n = \tilde{n}(m)$ in (72), we have $n + n_T = \tilde{n}(m+1)$ due to the definition of $T_{m+1} = t_{\tilde{n}(m+1)}$ in *Step 2* of Appendix B and

$$\begin{aligned} & \sup_{t \in I_m} |\bar{x}(t) - \tilde{x}^{\tilde{n}(m)}(t)| \\ & \leq C_e \left\{ \frac{\sqrt{M}L}{2} [b(\tilde{n}(m)) - b(\tilde{n}(m+1))] + \sup_{\tilde{n}(m) \leq k \leq \tilde{n}(m+1)} |\xi_k - \xi_{\tilde{n}(m)}| \right\} + \frac{\sqrt{M}a_{\tilde{n}(m)+1}}{2}. \end{aligned} \quad (73)$$

Suppose that the step size $\{a_n : n > n_0\}$ satisfies

$$C_e \frac{\sqrt{M}L}{2} [b(\tilde{n}(m)) - b(\tilde{n}(m+1))] + \frac{\sqrt{M}a_{\tilde{n}(m)+1}}{2} < \frac{\delta}{2}, \quad (74)$$

for $m \geq 0$.

Given $\sup_{t \in I_m} |\bar{x}(t) - \tilde{x}^{\tilde{n}(m)}(t)| > \delta$, we can obtain from (73) and (74) that

$$\begin{aligned} & \sup_{\tilde{n}(m) \leq k \leq \tilde{n}(m+1)} |\xi_k - \xi_{\tilde{n}(m)}| \\ & \geq \frac{1}{C_e} \left(\sup_{t \in I_m} |\bar{x}(t) - \tilde{x}^{\tilde{n}(m)}(t)| - \frac{\sqrt{M}L}{2} [b(\tilde{n}(m)) - b(\tilde{n}(m+1))] - \frac{\sqrt{M}a_{\tilde{n}(m)+1}}{2} \right) \\ & > \frac{1}{C_e} \left(\sup_{t \in I_m} |\bar{x}(t) - \tilde{x}^{\tilde{n}(m)}(t)| - \frac{\delta}{2} \right) \\ & > \frac{\delta}{2C_e}. \end{aligned}$$

Then, we get

$$\begin{aligned} & P \left(\sup_{t \in I_m} |\bar{x}(t) - \tilde{x}^{\tilde{n}(m)}(t)| > \delta \mid \sup_{t \in I_i} |\bar{x}(t) - \tilde{x}^{\tilde{n}(i)}(t)| \leq \delta, 0 \leq i < m \right) \\ & \leq P \left(\sup_{\tilde{n}(m) \leq k \leq \tilde{n}(m+1)} |\xi_k - \xi_{\tilde{n}(m)}| > \frac{\delta}{2C_e} \mid \sup_{t \in I_i} |\bar{x}(t) - \tilde{x}^{\tilde{n}(i)}(t)| \leq \delta, 0 \leq i < m \right) \\ & \stackrel{(a)}{=} P \left(\sup_{\tilde{n}(m) \leq k \leq \tilde{n}(m+1)} |\xi_k - \xi_{\tilde{n}(m)}| > \frac{\delta}{2C_e} \right), \end{aligned} \quad (75)$$

where step (a) is due to the independence of noise, i.e., $(\xi_k - \xi_{\tilde{n}(m)}), \tilde{n}(m) \leq k \leq \tilde{n}(m+1)$ are independent of $\hat{x}_n, n_0 \leq n \leq \tilde{n}(m)$.

The lower bound of the probability that the sequence $\{\hat{x}_n : n \geq n_0\}$ remains in the invariant

set \mathcal{I} is given by

$$\begin{aligned}
& P(\hat{x}_n \in \mathcal{I}, \forall n \geq n_0) \\
& \stackrel{(a)}{\geq} P\left(\sup_{t \in I_m} |\bar{x}(t) - \tilde{x}^{\tilde{n}(m)}(t)| \leq \delta, \forall m \geq 0\right) \\
& \stackrel{(b)}{\geq} 1 - \sum_{m \geq 0} P\left(\sup_{t \in I_m} |\bar{x}(t) - \tilde{x}^{\tilde{n}(m)}(t)| > \delta \mid \sup_{t \in I_i} |\bar{x}(t) - \tilde{x}^{\tilde{n}(i)}(t)| \leq \delta, 0 \leq i < m\right) \\
& \stackrel{(c)}{\geq} 1 - \sum_{m \geq 0} P\left(\sup_{\tilde{n}(m) \leq k \leq \tilde{n}(m+1)} |\xi_k - \xi_{\tilde{n}(m)}| > \frac{\delta}{2C_e}\right),
\end{aligned} \tag{76}$$

where step (a) is due to Lemma 1, step (b) is due to Lemma 4.2 in [44], and step (c) is due to (75).

With the increasing σ -fields $\{\mathcal{G}_n : n \geq n_0\}$ defined in Appendix A, we have for $n \geq n_0$,

- 1) $\xi_n = \sum_{m=n_0+1}^n a_m \hat{z}_m \sim \mathcal{N}(0, \sum_{m=n_0+1}^n \frac{a_m^2}{2\rho})$,
- 2) ξ_n is \mathcal{G}_n -measurable, i.e., $\mathbb{E}[\xi_n | \mathcal{G}_n] = \xi_n$,
- 3) $\mathbb{E}[|\xi_n|^2] = \sum_{m=n_0+1}^n \frac{a_m^2}{2\rho} < \infty$,
- 4) $\mathbb{E}[\xi_n | \mathcal{G}_m] = \xi_m$ for all $n_0 \leq m < n$.

Therefore, ξ_n is a Gaussian martingale with respect to \mathcal{G}_n . Letting $\eta = \delta_0$, $M_i = \xi_{\tilde{n}(m)+i} - \xi_{\tilde{n}(m)}$ and $k = \tilde{n}(m+1) - \tilde{n}(m)$ in Lemma 4, then we can obtain

$$\begin{aligned}
& P\left(\sup_{\tilde{n}(m) \leq k \leq \tilde{n}(m+1)} |\xi_k - \xi_{\tilde{n}(m)}| > \frac{\delta}{2C_e}\right) \\
& \leq 2 \exp\left\{-\frac{\delta^2}{8C_e^2 \text{Var}[\xi_{\tilde{n}(m+1)} - \xi_{\tilde{n}(m)}]}\right\} \\
& = 2 \exp\left\{-\frac{\rho\delta^2}{4C_e^2 [b(\tilde{n}(m)) - b(\tilde{n}(m+1))]} \right\}.
\end{aligned} \tag{77}$$

From (76) and (77), we have

$$\begin{aligned}
& P(\hat{x}_n \in \mathcal{I}, \forall n \geq n_0) \\
& \geq P\left(\sup_{t \in I_m} |\bar{x}(t) - \tilde{x}^{\tilde{n}(m)}(t)| \leq \delta, \forall m \geq 0\right) \\
& \geq 1 - 2 \sum_{m \geq 0} \exp\left\{-\frac{\rho\delta^2}{4C_e^2 [b(\tilde{n}(m)) - b(\tilde{n}(m+1))]} \right\}.
\end{aligned} \tag{78}$$

Assume that the step-size a_n satisfies

$$b(n_0) = \sum_{i>n_0} a_i^2 \leq C = \frac{\rho\delta^2}{4C_e^2}, \quad (79)$$

Then, we can use Lemma 5 and obtain

$$\frac{\exp\left\{-\frac{\rho\delta^2}{4C_e^2[b(\tilde{n}(m))-b(\tilde{n}(m+1))]\right\}}{b(\tilde{n}(m))-b(\tilde{n}(m+1))} \leq \frac{\exp\left\{-\frac{\rho\delta^2}{4C_e^2b(n_0)}\right\}}{b(n_0)},$$

for $b(\tilde{n}(m)) - b(\tilde{n}(m+1)) < b(\tilde{n}(m)) \leq b(n_0)$, which is due to the increasing property of (64).

Hence, we have

$$\begin{aligned} & \sum_{m \geq 0} \exp\left\{-\frac{\rho\delta^2}{4C_e^2[b(\tilde{n}(m))-b(\tilde{n}(m+1))]\right\} \\ & \leq \sum_{m \geq 0} [b(\tilde{n}(m)) - b(\tilde{n}(m+1))] \cdot \frac{\exp\left\{-\frac{\rho\delta^2}{4C_e^2b(n_0)}\right\}}{b(n_0)} \\ & = b(n_0) \cdot \frac{\exp\left\{-\frac{\rho\delta^2}{4C_e^2b(n_0)}\right\}}{b(n_0)} = \exp\left\{-\frac{\rho\delta^2}{4C_e^2b(n_0)}\right\}. \end{aligned} \quad (80)$$

As $C_e = e^{L(T+a_{n_0})}$, $b(n_0) = \sum_{i>n_0} a_i^2$, and a_n is given by (28), we can obtain

$$\frac{\rho\delta^2}{4C_e^2b(n_0)} = \frac{\delta^2}{4e^{2L(T+\frac{\alpha}{N_0+1})} \sum_{i \geq 1} \frac{1}{(i+N_0)^2}} \cdot \frac{\rho}{\alpha^2}. \quad (81)$$

In (81), $0 < \delta < \inf_{v \in \partial \mathcal{B}} |v - \hat{x}_{n_0}|$, (74) and (79) should be satisfied, where a sufficiently large $N_0 \geq 0$ can make both (74) and (79) true.

To ensures that $\hat{x}_{n_0} + a_{n_0+1}f(\hat{x}_{n_0}, x)$ does not exceed the mainlobe $\mathcal{B}(x)$, i.e., the first step-size a_{n_0+1} satisfies

$$|\hat{x}_{n_0} + a_{n_0+1}f(\hat{x}_{n_0}, x) - x| < \frac{\lambda}{Md},$$

we can obtain the maximum α as follows

$$\alpha_{\max} = \frac{(N_0 + 1) \left(|x - \hat{x}_{n_0}| + \frac{\lambda}{Md}\right)}{|f(\hat{x}_{n_0}, x)|}.$$

Hence, from (81), we have

$$\frac{\rho\delta^2}{4C_e^2b(n_0)} \geq C(\hat{x}_{n_0}) \triangleq \frac{\delta^2}{4e^{2L(T+\frac{\alpha_{\max}}{N_0+1})} \sum_{i \geq 1} \frac{1}{(i+N_0)^2}}. \quad (82)$$

Combining (78), (80) and (82), yields

$$\begin{aligned}
& P(\hat{x}_n \in \mathcal{I}, \forall n \geq n_0) \\
& \geq P\left(\sup_{t \in I_m} |\bar{x}(t) - \tilde{x}^{\tilde{n}(m)}(t)| \leq \delta, \forall m \geq 0\right) \\
& \geq 1 - 2e^{-C(\hat{x}_{n_0}) \cdot \frac{\rho}{\alpha^2}},
\end{aligned}$$

which completes the proof.

APPENDIX G

PROOF OF LEMMA 3

Apply the discrete Gronwall inequality [47], leading (61) to

$$|\bar{x}(t_{n+m}) - \tilde{x}^n(t_{n+m})| \leq Ce^{L \sum_{i=1}^m a_{n+i}}. \quad (83)$$

Since $1 \leq m \leq n_T$ and $n_T = \inf \{i \in \mathbb{Z} : t_{n+i} \geq t_n + T\}$, we get

$$\sum_{i=1}^m a_{n+i} = t_{n+m} - t_n \leq T + a_{n+n_T} \leq T + a_{n_0}. \quad (84)$$

By combining (83) and (84), we have

$$|\bar{x}(t_{n+m}) - \tilde{x}^n(t_{n+m})| \leq Ce^{L(T+a_{n_0})}. \quad (85)$$

For $\forall t \in [t_{n+m-1}, t_{n+m}]$, $1 \leq m \leq n_T$, from (49), we have

$$\begin{aligned}
\bar{x}(t) &= \bar{x}(t_{n+m-1}) + \frac{(t - t_{n+m-1}) [\bar{x}(t_{n+m}) - \bar{x}(t_{n+m-1})]}{a_{n+m}} \\
&= \gamma \bar{x}(t_{n+m-1}) + (1 - \gamma) \bar{x}(t_{n+m}),
\end{aligned}$$

where $\gamma = \frac{t_{n+m}-t}{a_{n+m}} \in [0, 1]$. Then, we can get (86) on the top of the next page, where step (a) is according to the definition of $\tilde{x}^n(t)$ in (50), step (b) is due to (85), step (c) is obtained from (69), and step (d) is obtained by using $\gamma = \frac{t_{n+m}-t}{a_{n+m}}$.

Therefore, from (86), we can obtain

$$\sup_{t \in [t_n, t_{n+n_T}]} |\bar{x}(t) - \tilde{x}^n(t)| \leq \frac{\sqrt{M}a_{n+1}}{2} + Ce^{L(T+a_{n_0})},$$

which completes the proof.

$$\begin{aligned}
& |\bar{x}(t) - \tilde{x}^n(t)| \\
&= |\gamma(\bar{x}(t_{n+m-1}) - \tilde{x}^n(t)) + (1 - \gamma)(\bar{x}(t_{n+m}) - \tilde{x}^n(t))| \\
&\stackrel{(a)}{=} \left| \gamma \left[\bar{x}(t_{n+m-1}) - \tilde{x}^n(t_{n+m-1}) - \int_{t_{n+m-1}}^t f(\tilde{x}^n(s), x) ds \right] \right. \\
&\quad \left. + (1 - \gamma) \left[\bar{x}(t_{n+m}) - \tilde{x}^n(t_{n+m}) - \int_{t_{n+m}}^t f(\tilde{x}^n(s), x) ds \right] \right| \\
&\leq \gamma \left| \int_{t_{n+m-1}}^t f(\tilde{x}^n(s), x) ds \right| + (1 - \gamma) \left| \int_{t_{n+m}}^t f(\tilde{x}^n(s), x) ds \right| \\
&\quad + \gamma |\bar{x}(t_{n+m-1}) - \tilde{x}^n(t_{n+m-1})| + (1 - \gamma) |\bar{x}(t_{n+m}) - \tilde{x}^n(t_{n+m})| \\
&\stackrel{(b)}{\leq} \gamma \int_{t_{n+m-1}}^t |f(\tilde{x}^n(s), x)| ds + (1 - \gamma) \int_t^{t_{n+m}} |f(\tilde{x}^n(s), x)| ds + Ce^{L(T+a_{n_0})} \\
&\stackrel{(c)}{\leq} \sqrt{M}\gamma(t - t_{n+m-1}) + \sqrt{M}(1 - \gamma)(t_{n+m} - t) + Ce^{L(T+a_{n_0})} \\
&\stackrel{(d)}{\leq} 2\sqrt{M}a_{n+m}\gamma(1 - \gamma) + Ce^{L(T+a_{n_0})} \leq \frac{\sqrt{M}a_{n+m}}{2} + Ce^{L(T+a_{n_0})} \\
&\leq \sup_{1 \leq m \leq n_T} \frac{\sqrt{M}a_{n+m}}{2} + Ce^{L(T+a_{n_0})} = \frac{\sqrt{M}a_{n+1}}{2} + Ce^{L(T+a_{n_0})}.
\end{aligned} \tag{86}$$

APPENDIX H

PROOF OF LEMMA 4

As M_i is a Gaussian martingale in i and the exponential function is positive and convex, e^{CM_i} is a positive submartingale for any $C \geq 0$. By utilizing the Doob's inequality [48] for $\eta > 0$, we have

$$P \left(\sup_{0 \leq i \leq k} M_i > \eta \right) \leq \frac{\mathbb{E} [e^{CM_k}]}{e^{C\eta}}.$$

Due to the property of Gaussian distribution, we have

$$\mathbb{E} [e^{CM_k}] = \exp \left\{ \frac{C^2}{2} \text{Var} [M_k] \right\}.$$

Then we can obtain

$$P \left(\sup_{0 \leq i \leq k} M_i > \eta \right) \leq \exp \left\{ \frac{C^2}{2} \text{Var} [M_k] - C\eta \right\}.$$

We choose the C to minimize the upper bound above, which yields $C = \frac{\eta}{\text{Var}[M_k]}$. Therefore, we

have

$$P\left(\sup_{0 \leq i \leq k} M_i > \eta\right) \leq \exp\left\{-\frac{\eta^2}{2 \operatorname{Var}[M_k]}\right\}.$$

Because the distribution of $\{M_1, M_2, \dots, M_k\}$ is symmetric, we get

$$\begin{aligned} & P\left(\sup_{0 \leq i \leq k} |M_i| > \eta\right) \\ &= P\left(\sup_{0 \leq i \leq k} M_i > \eta \bigcup \inf_{0 \leq i \leq k} M_i < -\eta\right) \\ &\leq P\left(\sup_{0 \leq i \leq k} M_i > \eta\right) + P\left(\inf_{0 \leq i \leq k} M_i < -\eta\right) \\ &= 2P\left(\sup_{0 \leq i \leq k} M_i > \eta\right). \end{aligned}$$

Hence, we have

$$P\left(\sup_{0 \leq i \leq k} |M_i| > \eta\right) \leq 2 \exp\left\{-\frac{\eta^2}{2 \operatorname{Var}[M_k]}\right\},$$

which completes the proof.